Preparation and characterization of multi-component tablets containing co-amorphous salts : Combining multimodal non-linear optical imaging with established analytical methods

Ojarinta, Rami

2018-11

Ojarinta , R , Saarinen , J , Strachan , C J , Korhonen , O & Laitinen , R 2018 , ' Preparation and characterization of multi-component tablets containing co-amorphous salts : Combining multimodal non-linear optical imaging with established analytical methods ' , European Journal of Pharmaceutics and Biopharmaceutics , vol. 132 , pp. 112-126 . https://doi.org/10.1016/j.ejpb.2018.09.013

http://hdl.handle.net/10138/308342
https://doi.org/10.1016/j.ejpb.2018.09.013

Preparation and characterization of multi-component tablets containing co-amorphous salts: combining multimodal non-linear optical imaging with established analytical methods

Rami Ojarinta[a,*], Jukka Saarinen[b], Clare J. Strachan[b], Ossi Korhonen[a], Riikka Laitinen[a]

[a] School of Pharmacy, University of Eastern Finland, P.O. Box 1627, 70211 Kuopio, Finland

[b] Drug Research Program, Division of Pharmaceutical Chemistry and Technology, Faculty of Pharmacy, University of Helsinki, Viikinkaari 5 E, 00014 University of Helsinki, Finland

*Corresponding author:

Tel. +358 40 355 3870

E-mail: rami.ojarinta@uef.fi

ABSTRACT

Co-amorphous mixtures have rarely been formulated as oral dosage forms, even though they have been shown to stabilize amorphous drugs in the solid state and enhance the dissolution properties of poorly soluble drugs.

In the present study we formulated tablets consisting of either spray dried co-amorphous ibuprofen-arginine or indomethacin-arginine, mannitol or xylitol and polyvinylpyrrolidone K30 (PVP). Experimental design was used for the selection of tablet compositions, and the effect of tablet composition on tablet characteristics was modelled. Multimodal non-linear imaging, including coherent anti-Stokes Raman scattering (CARS) and sum frequency/second harmonic generation (SFG/SHG) microscopies, as well as scanning electron microscopy, X-ray diffractometry and Fourier-transform infrared spectroscopy were utilized to characterize the tablets.

The tablets possessed sufficient strength, but modelling produced no clear evidence about the compaction characteristics of co-amorphous salts. However, co-amorphous drug-arginine mixtures resulted in enhanced dissolution behaviour, and the PVP in the tableting mixture stabilized the supersaturation. The co-amorphous mixtures were physically stable during compaction, but the excipient selection affected the long term stability of the ibuprofen-arginine mixture. CARS and SFG/SHG proved feasible techniques in imaging the component distribution on the tablet surfaces, but possibly due to the limited imaging area, recrystallization detected with x-ray diffraction was not detected.

KEYWORDS: Co-amorphous, amino acid, tablet, deformation, dissolution, multimodal non-linear imaging, CARS, SFG, SHG

ABBREVIATIONS[1]

[1] ACN, acetonitrile; ARG, arginine; CA, co-amorphous; CARS, coherent anti-Stokes Raman scattering; ER%, elastic recovery (%); FTIR, Fourier-transform infrared spectroscopy; HPLC, high-performance liquid chromatography; IBU, ibuprofen; IND, indomethacin; IR, infrared; KL, Kuentz-Leuenberger; PM, physical mixture; PVP, polyvinylpyrrolidone K30; SD, spray drying; SEM, scanning electron microscopy; SFG, sum frequency generation; TFA, trifluoro acetic acid; XRD, X-ray diffraction

1. INTRODUCTION

The majority of drugs currently under development possess poor water solubility, which may lead to limited oral bioavailability as well as challenges in drug formulation and *in vitro* and *in vivo* testing during drug development [1,2]. Transformation of a crystalline drug to the amorphous form is a promising option for overcoming these challenges, since it has been shown to effectively increase the apparent solubility and dissolution rate of poorly soluble drugs [3-5]. However, the use of amorphous drugs has been limited due to their poor physical stability (i.e. tendency to recrystallize).

To stabilize the amorphous form, different glass solution subtypes, i.e. polymeric amorphous solid dispersions, mesoporous silicon or silica-based glass solutions, and co-amorphous formulations have been introduced [4-9]. Of these formulations, the solid dispersions are the most extensively studied, but during the last decade the interest towards co-amorphous formulations (i.e. single-phase amorphous mixtures of the drug and two or more pharmaceutically active or inactive low molecular weight substances) has increased due to the potential for good physical stability, combination therapy and the reduced size of the final dosage form [4,7-10]. Additionally, co-amorphous formulations (especially co-amorphous salts) have been shown to increase dissolution rates, and in some studies even stabilize supersaturation, when compared to the crystalline or, more importantly, to the pure amorphous drugs [9-13].

Being a relatively novel formulation approach, the co-amorphous mixtures have mainly been prepared by small scale methods, but in recent years also preparation methods that can be scaled up, such as spray drying (SD) and hot-melt extrusion, have been successfully utilized [9,14-19]. However, even though the co-amorphous systems are generally developed to improve the oral bioavailability, the development of oral dosage forms containing co-amorphous mixtures is still in its infancy [10,20]. Recently, some authors have successfully included co-amorphous mixtures in tablet formulations [21-23], but the deformation properties of the co-amorphous mixtures and the

effect of tablet composition on tablet properties has remained unexplored, even though the compaction properties of the co-amorphous components may differ from their crystalline counterparts and the excipients may significantly affect the deformation properties, mechanical strength, drug release as well as physical stability of the amorphous components [24-27]. Additionally, both Lenz et al. [21] and Petry et al. [22] investigated the physical stability of co-amorphous indomethacin-arginine (IND-ARG) from ground tablets with conventional methods (X-ray diffraction (XRD), Fourier-transform infrared spectroscopy (FTIR)), even though the recrystallization may be more pronounced on the tablet surface, and it may be too otherwise limited to be observed with conventional methods [27,28].

Non-linear optical imaging techniques, including coherent anti-Stokes Raman scattering (CARS) and sum frequency/second harmonic generation (SFG/SHG) microscopies, are relatively new imaging modalities with interesting capabilities. The general benefits of these techniques include label-free, chemically-specific signal, fast data-acquisition time and inherent non-destructive "confocal"- like imaging [29]. The label-free nature of CARS is based on the non-linear probing of molecular vibrational resonances [30], whereas materials with non-centrosymmetric structures generate SFG/SHG signals [31]. Most of the research in the use of non-linear optics has been focused on instrument development, however studies of the applications of non-linear optical imaging in different fields are increasing. Mostly, these techniques have been used in biomedical applications, where especially CH_2 stretching of lipids has been probed with CARS [32], while collagen has been imaged with SHG [33]. However, pharmaceutical applications including solid-state analysis of non-linear optical imaging have also been increasing [29]. For example CARS has been used to identify solid-state forms of IND on tablet surfaces [34,35] and to monitor the solid-state changes of theophylline during dissolution [36]. On the other hand SFG/SHG, can be especially useful in solid-state analysis, since only non-centrosymmetric crystals produce SFG/SHG signals. SHG has been quantitatively used to analyse pharmaceutical solid-solid mixtures [37] and

has also been utilized in imaging, for example to visualize trace crystallinity in powder mixtures with a detection limit of 4 ppm [38]. In multimodal non-linear optical imaging, CARS and SFG/SHG can be simultaneously combined. It was recently shown that such a combination is well-suited to the detection of different polymorphs and the amorphous form on tablet surfaces with high sensitivity [35]. Crystallisation processes during storage can be imaged in detail. While in that study tablets were composed of pure drug, the multimodal technique also has much potential for analysing relatively complex multicomponent tablets. Multimodal CARS and SFG/SHG imaging has not yet been used to image formulations containing both drug and excipient, nor changes in their crystallinity and component distribution upon storage.

In the present study, we prepared tablets containing amorphous salts of ibuprofen (IBU) and ARG and IND and ARG, and employed multi-modal non-linear optical imaging and established analytical methods to explore the effect of formulation variables on pharmaceutical performance. The tablet compositions were selected with an experimental design that consisted of three factors, i.e. the amount of drug-ARG salt, the amount of polyvinylpyrrolidone K30 (PVP) and the sugar alcohol species. Our aim was to investigate the effect of the abovementioned variables on the compaction characteristics, on the mechanical properties of the tablets as well as on the drug release behaviour and the physical stability of the co-amorphous salts. Additionally, CARS and SFG/SHG were combined in order to explain compaction properties by visually detecting the drug and excipient distribution and to detect possible phase separation and re-crystallization on the surface of complex multi-component tablets during storage.

2. MATERIALS AND METHODS

2.1 Materials

ARG (L-enantiomer) and PVP were purchased from Sigma-Aldrich Co. (St. Louis, USA) and γ-IND from Hangzhou Dayanchem (Hangzhou, China). Racemic R,S-IBU and the sugar alcohols

(mannitol (Pearlitol® 200SD) and xylitol (Xylisorb® 200DC)) were kindly donated by Orion Corporation (Espoo, Finland) and Roquette (Lestrem, France), respectively. Glacial acetic acid (Riedel de Haën, Seelze, Germany), hydrochloric acid (HCl, 37 %; Riedel-de-Haën, Seelze, Germany), potassium chloride (J. T. Baker, Deventer, Holland), sodium acetate (Riedel-de-Haën, Seelze, Germany), sodium hydroxide (NaOH; VWR Chemicals, Leuven, Belgium), and potassium dihydrogen phosphate (KH_2PO_4; Merck, Darmstadt, Germany) were used in the preparation of the buffer solutions. During the storage of the samples, dry conditions were maintained with phosphorus pentoxide (P_2O_5), while approximately 33% RH was maintained with saturated magnesium chloride ($MgCl_2$) solution. Ultrapurified water (class I; Elga Purelab Ultra, Elga LabWater, UK) was used in the high-performance liquid chromatography (HPLC) mobile phase as well as to prepare the drug-ARG solutions prior to the SD. Otherwise class II water (Elix 5, Millipore S.A.S., Molsheim, France) was used throughout the study. Acetonitrile (ACN; HPLC grade; VWR Chemicals, Leuven, Belgium and Fisher Chemical, Loughborough, UK) and trifluoro acetic acid (TFA; HPLC-grade; Sigma-Aldrich, Germany) were the other components of the high performance liquid chromatography (HPLC) mobile phase.

2.2 Methods

2.2.1 Preparation of the co-amorphous salts

The co-amorphous IBU-ARG and IND-ARG salts were prepared by spray drying as described in our previous article [19]. Briefly, an amount of drug was dissolved in a corresponding amount of 5% ARG-water solution in order to obtain a drug-ARG molar ratio of 1:1, and once the solution was visually clear, it was spray dried with a Büchi Mini Spray Dryer B-191 (Büchi Labortechnik AG, Flawil, Switzerland). The water content of the freshly prepared samples was measured in triplicate with a coulometric Karl-Fischer titrator (Mettler Toledo C30, Mettler-Toledo GmbH, Greifensee, Switzerland). After preparation, the co-amorphous systems were stored in brown glass jars under 4 °C 0% RH conditions until the tablets were prepared.

2.2.2 Tablet composition and experiment design

The tablet mixture compositions (Table 1) were based on a 2-level full factorial experiment design with three centre points that was conducted with Modde Pro-software (11.0.1, MKS Umetrics AB, Sweden). The experimental factors were drug load, amount of PVP, and the sugar alcohol species, whereas the responses were tablet tensile strength, elastic recovery, 1/*C*-value from the Kuentz-Leuenberger (KL) equation (Eq. 3, see section 2.2.5), the cumulative dissolved amount of drug after 15 min (CDA_{15min}), and the area under the cumulative dissolved drug amount-time curve after the 2h dissolution study ($AUC_{0\text{-}120min}$). The compaction force and the relative amount of the sugar alcohol were kept constant (20 kN and 60% (m/m) of the tablet mass, respectively). Thus, the tablet mass was changed according to the drug dose and the amount of PVP.

2.2.3 Preparation of the powder mixtures

The powder blends for tableting were prepared in a mortar by first mixing the drug-ARG mixture with PVP and then adding the sugar alcohol in two or three batches depending on the amount of the final mixture. The homogeneities of the prepared powder mixtures were investigated with two model formulations (B4 and N2) by dissolving five parallel tablets in 250 ml of phosphate buffer (pH 7.4) in ambient conditions and analysing the drug content with HPLC after 24h.

2.2.4 Tablet preparation

Flat faced tablets (diameter 13 mm) were compressed with a compaction simulator (PCS-1, PuuMan Ltd., Kuopio, Finland) using a double-sided sine wave compression profile (duration 1500 ms). Due to high ejection forces, powder sticking and tablet fracturing occurred during preliminary studies without lubrication, and thus magnesium stearate was added to the die walls and lower punch using a brush prior to every compression except for the tablets for stability studies. The compaction force was set to approximately 20 kN with every formulation. The tablets were weighed immediately after compression, whereas the dimensions were measured the next day.

2.2.5 Compaction characteristics

The force-displacement data of five parallel compressions were collected and corrected according to the punch deformations. This corrected data was utilized to determine the relative density (ρ) of the different formulations at various compaction pressures according to Eq. 1:

$$\rho = \frac{\rho_{app}}{\rho_{t,mix}} \tag{1}$$

where ρ_{app} is the density at a certain pressure and $\rho_{t,mix}$ is the true density of the formulation that was calculated according to Eq. 2:

$$\rho_{t,mix} = \frac{w_1 + \cdots + w_n}{\frac{w_1}{\rho_{t1}} + \cdots + \frac{w_n}{\rho_{tn}}} \tag{2}$$

Here, w denotes weight fraction and ρ_t the true density, while the subscripts 1 and n refer to the different components of the formulation [40]. The ρ_t-values of the single components were obtained from the literature [41-43].

The deformation properties of the different formulations were evaluated using the KL-equation (Eq. 3):

$$\sigma = \frac{1}{C}\left[\rho_c - \rho - (1-\rho_c)\ln\left(\frac{1-\rho}{1-\rho_c}\right)\right] \tag{3}$$

where σ is the compaction pressure, $1/C$ is a plasticity parameter (interpretation corresponds to the yield pressure from Heckel equation) and ρ_c is the critical relative density (relative density where mechanical rigidity emerges in the powder bed) [44,45]. To determine the ρ_c, the pressure susceptibility (χ_p; susceptibility of the powder bed to external pressure) at each data point was calculated using Eq. 4 after which the χ_p was plotted against relative density as described by Kuentz and Leuenberger [44]. The ρ_c was considered as the pressure where the χ_p began to systematically decrease with increasing ρ (an example shown in the supplementary material (Figures S1A and S1B)). Finally, the constant C was obtained by fitting Eq. 3 to the σ vs. ρ data (Figure S1C) using

nonlinear regression that was conducted with SigmaPlot 14.0 (Systat Software Inc., San Jose, CA, USA).

$$\frac{d\rho}{d\sigma} = \chi_p(1-\rho) \quad (4)$$

The percentage of axial elastic recovery (*ER%*) was obtained by using Eq. 5 [46]:

$$ER\% = \frac{H - H_c}{H_c} \times 100\% \quad (5)$$

where H is the tablet height measured 24h after compression and H_c is the tablet height at maximum pressure.

A universal tester (CT-5 tester, Engineering Systems, Nottingham, England) was used to determine the crushing strengths of the tablets (n = 5) 24h after the compression. The tensile strengths (σ) were calculated according to Eq. 6:

$$\sigma = \frac{2P}{\pi D t} \quad (6)$$

where P is the applied load (crushing strength), D is the tablet diameter, and t is the tablet thickness [47].

2.2.6 Dissolution studies

The dissolution studies were performed with Sotax AT6 and Sotax AT7 smart dissolution testers (Sotax AG, Basel, Switzerland) equipped with paddle stirrers. Each tablet formulation was studied in triplicate in 500 ml of dissolution medium (pH 1.2 HCl buffer for IBU-tablets and pH 5.0 acetate buffer for IND tablets) that was kept at 37 °C and stirred at 50 rpm. The duration of the study was 2 hours, the samples were taken at 5 min, 10 min, 15 min, 30 min, 60 min, 90 min, and 120 min time points, and the sample volume (5 ml) was replaced with buffer solution. The samples were filtered through 0.22 µm membrane filters (Syringe filter 30 mm Dia, PES 0.22 µm Membrane, Sterile,

Porvair Sciences, Leatherhead, UK), and the drug concentration was analysed with HPLC (see section 2.2.7). Prior to the HPLC analysis, the samples were diluted with ACN to reach ACN/H_2O-ratio of 70/30, and if necessary, further dilution was conducted with 70/30 ACN/H_2O mixture to obtain drug concentrations below 100 µg/ml.

The effect of the formation of amorphous state and the effect of ARG on the dissolution behaviour of the drugs were investigated by performing the 2h dissolution studies with tablets corresponding to B4 and N2 formulations but containing either physical mixtures of the crystalline drug and ARG or only the crystalline drug (ARG replaced by mannitol) instead of the co-amorphous salt. Additionally, to investigate the effect of PVP on the supersaturation stability of the co-amorphous salts, a 24h dissolution study was conducted with B4- and N2-formulations as well as with formulations corresponding to B4 and N2, but in which the PVP was replaced with excess mannitol. In these studies, the samples were taken at 5 min, 10 min, 15 min, 30 min, 1 h, 2 h, 4 h, 6 h, 8 h and 24 h time points.

2.2.7 HPLC

The HPLC equipment consisted of Gilson 321 pump and Gilson UV-vis 151 detector (Gilson Inc., Middleton, WI, USA), Gilson 234 auto injector (Gilson, Roissy-en-France, France), and a reversed phase column (Phenomenex Gemini NX 5u C18 110A, 250x4, 60 mm, sr. nr. 590531-19, USA) with a pre-column. The mobile phase (70/30 ACN/H_2O acidified with 0.1% TFA) flow rate was 1.2 ml/min and the detection wavelengths were 221 nm for IBU and 225 nm for IND. The standard solutions (1, 5, 25, 50, 75, and 100 µg/ml) were prepared in 70/30 ACN/H_2O-mixture and measured with HPLC to obtain standard lines that were linear ($R^2 > 0.997$) in the examined concentration range.

2.2.8 Tablet characterization

The tablet formulations were stored under 25 °C/33% RH to investigate the effect of compaction and tablet composition on the physical stability of co-amorphous salts. XRD and FTIR were used as standard methods to detect re-crystallization during the 20-week test period.

X-ray diffractograms were collected from intact tablet surfaces using a Bruker D8 Discover diffractometer (Bruker AXS GmbH, Karlsruhe, Germany) with Cu Kα radiation (λ = 1.54 Å) and a motorized slit. An acceleration voltage of 40 kV and current of 40 mA were used to perform a scan between 5 and 35° 2θ with a scan speed of 0.1 s/step and step size of 0.011°. DIFFRAC.V3-software (Bruker AXS GmbH) was utilized for data collection.

The attenuated total reflectance (ATR) FTIR measurements were conducted with Thermo Nicolet Nexus 8700 spectrometer (Thermo Electron Corp., Madison, WI, USA) and with Nicolet iS50 FT-IR spectrometer (Thermo Scientific, Madison, WI, USA). The spectra were collected over a wavenumber range of 650-4000 cm^{-1} as an average of 64 scans with the resolution of 4 cm^{-1}. OMNIC-software (Thermo Scientific) was used for data collection and analysis.

Additionally, CARS and SFG/SHG microscopies were utilized as more novel non-linear imaging methods to characterize the raw materials and to detect phase separation and recrystallization on the tablet surface as well as to image the drug-excipient distribution on the tablet surface. A Leica TCS SP8 CARS microscope (Leica Microsystems, Wetzlar, Germany) was used. Briefly, the imaging system consisted of an inverted microscope with a laser-scanning confocal scan-head and photomultiplier tube (PMT) and GaAsP hybrid (HyD) photodetectors. The Stokes beam (ω_S) for CARS excitation was emitted from a Nd:YVO_4 solid-state laser (1064.5 nm) (picoEMERALD®, APE, Berlin, Germany). Laser source was integrated with an optical parametric oscillator (OPO) that generated tunable pump/probe beams (ω_p and ω_{pr}).The bandwidth of the Stokes beam (ω_S) was about 2-3 cm^{-1} and the repetition rate was 80 MHz. The pulse duration was 7 ps for the Stokes and 5-6 ps for the pump (ω_p) and probe beams (ω_{pr}). The pump beam wavelength can be tuned so that the energy difference between these beams corresponds to some molecular vibrational resonance.

The vibration is then probed with a probe photon, which can originate from the same beam as the pump photon. These beams are coherently driven into the sample and wave mixing results in generation of the fourth, blue-shifted, anti-Stokes photon (ω_{as}), which is then detected. A water-immersion objective (25× 0.95 NA) HCX IRAPO L (Leica) was used to focus the light onto the sample that was placed on a microscope slide No. 1.5. Epi-CARS detection was used to collect anti-Stokes signal using a nondescanned PMT detector, while another nondescanned PMT detector was simultaneously used to collect epi-directed SFG/SHG signals with the bandpass filter 465 nm ± 85 nm. HeNe laser (633 nm) was also used to visualize the tablet surfaces as reflected light was detected with a PMT detector. Images of 512 × 512 or 1024 × 1024 pixels were acquired with a pixel dwell time of 1.2 µs (scanning speed 400 Hz, line average 2). For the spectroscopic analysis, the wavelength of the pump beam was systematically changed 33 times from 893 nm to 925 nm covering the CARS shifts between 1804 cm^{-1} and 1417 cm^{-1}. The acquisition time for each spectral scan was approximately 15 mins. CARS spectra in the figures are offset for clarity. Contrast was adjusted individually for each image. The Leica Application Suite Advanced Fluorescence (LASAF) was used for image acquisition and processing together with Fiji ImageJ (open-source distribution), GNU Image Manipulation Program v2 (open-source distribution) and Origin 2018 (OriginLab, Northampton, Massachusetts, USA). RGB color images based on PCA were generated as described elsewhere using MATLAB R2016a (MathWork, MA, USA) [35]. Briefly, spectral data was mean centered and SNV corrected and the PC score values were normalized so that the minimum PC score value was set to 0 and the maximum score value to 1 and all values in between scaled linearly. PC1, PC2, and PC3 scores are represented by red, green, and blue coloring, respectively.

To verify the morphological aspects observed with CARS, the fresh and stored (6 months) tablets as well as the spray dried drug-ARG powders were imaged with scanning electron microscopy (SEM). The morphology of the spray dried particles was micrographed with a field emission scanning

electron microscope (Zeiss Sigma HD VP, Carl Zeiss NTS, Cambridge, UK) using Everhart-Thornley type secondary electron detector and a 30 µm aperture in high vacuum with acceleration voltage of 4 kV. With the tablets, the images were obtained under low vacuum conditions (15 Pa chamber pressure with dry nitrogen gas) with a VPSE G3 detector (Carl Zeiss NTS, Cambridge, UK) and an acceleration voltage of 10 kV. The low vacuum (higher gas pressure) conditions were used with the tablets, because the tablet height (2-3 mm) and the porous structure of the tablets including microfractures decreased the electric conductivity of the specimen. The charge due to the electron beam was eliminated with the nitrogen gas medium.

2.2.9 Statistical analysis

The effect of the selected tablet composition variables (factors) on the tablet properties (responses) were investigated with multiple linear regression (MLR) using MODDE Pro-software (11.0.1, MKS Umetrics AB, Sweden). A separate model was created for each response, and the non-significant interaction terms were excluded to provide the best possible model. The goodness of fit (R^2) and goodness of prediction (Q^2) were utilized to evaluate the models. In a good model, R^2 should gain values close to 1, whereas a Q^2 above 0.5 indicates good predicting power [48,49].

GraphPad Prism 5.03 (GraphPad Software Inc., La Jolla, USA) was used for the determination of the $AUC_{0\text{-}120min}$s and to conduct single-factor ANOVA with Tukey's post-hoc test. The results of the statistical analyses were considered significant if $p < 0.05$.

3. Results and discussion

3.1 Tablet preparation

3.1.1 Spray drying

The spray drying of IBU-ARG solution resulted in white and loosely packed powder, whereas the spray dried IND-ARG powder was yellow and slightly denser packed. Both of the powders were

299 rather cohesive and non-free flowing and, according to the SEM images (Figure 1), the spray dried
300 particles were spherical in shape and possessed diameters from less than 1 μm to a few dozens of
301 micrometres, which is typical for spray dried materials [50]. The average yields of the spray drying
302 were 31% with IND-ARG and 42% with IBU-ARG, which were similar with the values of our
303 recent study (29.2%-34.4% [19]) but lower than the yield reported by Jensen et al. (~70% [16]).
304 Additionally, the moisture contents of the freshly prepared powders (2.8±0.6% (IBU-ARG) and
305 3.3±0.2% (IND-ARG)) were close to those reported previously for spray-dried IND-amino acid
306 mixtures (3-4% [16]), and this amount of water is probably due to the water reuptake from the
307 environment rather than incomplete drying, since similar values were also measured from ball-
308 milled samples [16].

309 *3.1.2 Preparation of the powder mixtures and tablet compaction*

310 The prepared drug-ARG-PVP-sugar alcohol mixtures were homogenous, at least in terms of drug
311 content (tested with B4- and N2-formulations), since relative standard deviations of the released
312 drug amounts between the parallel tablets were 5.7% with B4 and 4.0% with N2. However, neither
313 of the formulations released the full drug dose (84% and 91% released from B4 and N2,
314 respectively). The discrepancy between the theoretical drug content and actual released drug
315 amount from B4 and N2 formulations may indicate that the poor flow properties of the spray dried
316 mixtures resulted in challenges in the mixing process, i.e. sticking of the drug-ARG mixtures onto
317 the weighing boats, mixing cards and onto the rough mortar surfaces, rather than uneven drug-ARG
318 distribution in the powder mixture. Lenz et al. [21] avoided this challenge with spray dried IND-
319 ARG by combining it in a premixture with colloidal silicon dioxide that improved the powder flow
320 properties and probably decreased the surface adherence of IND-ARG. However, the additional
321 formulation components might have overcomplicated the analyses performed in the present study,
322 and thus, no premixture was prepared.

323 **3.2 Tablet properties**

3.2.1 Mechanical properties

The exact values for variables describing the mechanical properties of the different formulations are presented in the supplementary material (Table S1). The tablets containing IND-ARG (N-formulations) were slightly stronger than those containing IBU-ARG (B-formulations), but between corresponding formulations the difference was statistically significant only with pairs B3-N1 and B8-N4. With elastic recovery, no clear trend could be seen between the B and N formulations. The plasticity parameter (1/C) was significantly higher with every N formulation when compared to the corresponding (i.e. B1-N5, B2-N6, B3-N1, B4-N2, B5-N7, B6-N8, B7-N3, B8-N4) B formulations. Also, the ρ_c values were slightly higher with IND-ARG formulations, but since the same value was used for every parallel tablet, no statistical analysis could be made.

The tensile strengths (1.9-3.5 MPa; Table S1) of the tablets produced in the present study with a compaction force of 20 kN (compaction pressure ~150 MPa) were in agreement with observations of Lenz et al. [21], who reported tensile strengths of 2.0 and 4.5 MPa for tablets consisting of spray dried IND-ARG, mannitol, croscarmellose sodium, colloidal silicon dioxide and magnesium stearate that were compressed under pressures of 82.3 and 198.6, MPa respectively. The modelling of the effect of the tablet composition on tensile strength was challenging especially with B-formulations as indicated by summary of fit plots in the supplementary material (Figure S2), which can probably be explained by the low variation in tensile strength values together with the relatively large deviation between the parallel measurements. However, as observed also in previous research, mannitol formed stronger tablets than xylitol (Figure 2) [51]. Other main factors were insignificant. Additionally, despite the one significant interaction factor for the N-formulations (Figures 2 and 3 (1.)), the direction of the changes in tensile strength, caused by varied tablet composition, were well estimated by the significant main factor.

According to Tanner et al. [52], elastic recovery values between inelastic (e.g. glucose or calcium hydrogen phosphate) and highly elastic (e.g. starch) materials can vary from 1 to 18%. Thus, the

axial elastic recovery percentages obtained in the present study indicate that both B and N formulations possessed low or moderate elasticity. Additionally, even though elastic recovery as well as other compaction characteristics may depend not only on the material properties but also on the processing factors such as compaction force or speed, the elastic behaviour of the B and N formulations were in accordance with those reported for the single components [53-59].

The model characteristics R^2 and Q^2 (Figure S2) indicated that the modelling of the effect of tablet composition on the elastic recovery could be more successful than the modelling of tensile strength. The model prediction of decreasing elasticity with increasing amount of drug-ARG mixture (Figure 2) could be explained by the more efficient coverage of the excipient particles by the drug-ARG mixture, which could enhance particle bonding either by increased plasticity or adsorbance of water as observed with spray dried lactose [24,60]. However, due to the inconsistencies between the models of B and N formulations (opposite effect of sugar alcohol species on the ER% (Figure 2), no significant interactions in model for B formulations (Figure 2) vs. highly significant interactions with N formulations (Figures 2 and S3)), the conclusions concerning the effect of tablet composition on the elastic recovery must be made with caution.

In this study, the KL-equation was utilized instead of the widely used Heckel equation to evaluate the deformation properties due to its suggested better reliability [45]. According to R^2 and Q^2 values (Figure S2), the 1/C value could be modelled reliably for both B and N formulations. Additionally, the interaction plots (Figure 3 (2. and 3.)) indicated that the direction of the change in the 1/C value could be predicted reasonably well with the main factors. The sugar alcohol species had the most prominent effect on the 1/C value (Figure 2), which could again be expected due to their high proportion in the tablets. Xylitol resulted in lower 1/C values than mannitol, indicating higher plasticity [45]. This seems contradictory with previously reported deformation properties of primary mannitol and xylitol particles, but may be explained by sodium carboxymethyl cellulose (~2%) included in Xylisorb® 200DC, which lowered the yield pressure of metformin hydrochloride, when

co-spray dried with the drug [51,61]. In addition to the sugar alcohol species, both amount of drug-ARG mixture and amount of PVP affected the plasticity of the powder mixtures (Figure 2). The linear regression analyses between 1/C values of formulations containing low and high percentages (instead of absolute amounts) of drug-ARG mixture or PVP further indicated increased plasticity with an increasing proportion of drug-ARG mixture (slopes: -6.9 (B2-B5), -0.04 (B4-B7), -8.0 (N2-N3) and -3.2 (N6-N7)) and a decrease in plasticity with an increase in the proportion of PVP (slopes: 6.9 (B2-B5), 0.04 (B4-B7), 7.9 (N2-N3) and 3.1 (N6-N7)). The effect of drug-ARG amount on plasticity was consistent with previous studies in which plasticity increased with amorphous components [24,62-64], but the increase in the plasticity with the decrease in the amount of PVP was inconsistent with its previously reported plastic nature [65]. However, in the present study, the increase PVP proportion accompanied a decrease in the amount of the apparently plastic drug-ARG mixture, which may explain the inconsistency.

3.2.2 Dissolution properties

The cumulative amount of dissolved drug increased up to 30 min, after which it remained steady or began to decrease (Figure 4). None of the B-formulations released the full drug dose, whereas with the N-formulations six out of nine tablets exhibited over 90% drug release.

The CDA_{15min} and $AUC_{0\text{-}120min}$ values of the different formulations are presented in the supplementary material (Table S2). Since the B formulations were unable to release the full drug dose, there was only limited deviation between the $AUC_{0\text{-}120min}$ values of the B-formulations. However, the deviation was more pronounced in the CDA_{15min} value between B formulations as well as in both $AUC_{0\text{-}120min}$ and CDA_{15min} values between the N formulations. Thus, only a rather poor model (Q^2-value 0.23) could be formed to predict the effect of different factors on the $AUC_{0\text{-}120}$ of the B-formulations (not further analysed) but modelling of the CDA_{15min} of B formulations as well as $AUC_{0\text{-}120min}$ and CDA_{15min} of N formulations was more successful (Q^2-values of 0.58, 0.75

398 and 0.82, respectively (Figure S4)). As with the models predicting the mechanical properties, most
399 of the interaction plots (Figure 5) of the $AUC_{0\text{-}120}$ and CDA_{15min} models revealed that the direction
400 of the change in the response could be predicted by the main coefficients, but the magnitude of the
401 change may be dependent on another interacting factor.

402 According to the model, the amount of drug-ARG mixture and PVP were the most prominent
403 factors affecting the $AUC_{0\text{-}120min}$ and CDA_{15min} of the N-formulations (Figure 6). The increase in
404 $AUC_{0\text{-}120min}$ by increasing the IND-ARG amount was expected, since this factor described the drug
405 load instead of relative drug amount. Surprisingly, the model showed a negative effect of increasing
406 amount of PVP on both $AUC_{0\text{-}120min}$ and CDA_{15min}, even though PVP has been reported to enhance
407 the dissolution properties and stabilize the supersaturation of IND both freely in solution and in
408 solid dispersions [66-68], and, also in the present study, the ability of PVP to stabilize the
409 supersaturation of IND was clearly demonstrated in the 24h dissolution test with N2 formulations
410 containing and lacking PVP (Figure 7D). Some authors have, however, reported decreased
411 dissolution with amorphous solid dispersions with high PVP-IND ratios when compared to a
412 formulations with low PVP-IND ratio [69,70]. This phenomenon was attributed to increased
413 viscosity, which may have also reduced the IND release in the present study. With the B
414 formulations, the amount of IBU-ARG had no significant effect on the CDA_{15min}, probably due to
415 the incomplete drug release. According to the model, an increase in the amount of PVP, however,
416 significantly increased the CDA_{15min} of the B formulations suggesting the positive effect of PVP on
417 IBU release, which has been reported previously [71].

418 The drug release from formulations containing co-amorphous mixtures was faster than from
419 formulations containing physical drug-ARG mixture or plain crystalline drug, even though ARG in
420 the physical mixtures also enhanced drug release (Figure 7A and B). Additionally, with the N2-
421 formulation, the presence of ARG and the formation of an amorphous system significantly
422 increased the cumulative dissolved amount of IND at the end of the dissolution study (7.7%, 57.0%

423 and 92.7% drug release from tablets containing plain IND, physical IND-ARG mixture and co-
424 amorphous IND-ARG salt, respectively). The drug release was highest also from the B2
425 formulation containing co-amorphous IBU-ARG (45.2%), but there was no significant difference in
426 the amount of released drug between tablets containing physical mixture or crystalline IBU (31.9%
427 and 25.5%, respectively). The enhanced IBU and IND dissolution upon formation of the co-
428 amorphous system has been attributed to both its amorphous nature as well as salt formation
429 between the acidic drug and basic ARG [11,16,19,72]. With IND-ARG, enhanced drug release also
430 from the tablet formulation has been observed previously [21]. However, in our previous study [19],
431 the IND-ARG physical mixture (crystalline components) and γ-IND seemed to result in similar
432 dissolution profiles, whereas in the present study, drug release was higher with the physical
433 mixture. This may be due to the *in situ* amorphization of IND-ARG, which has been previously
434 observed to occur in tablets containing an IND-ARG physical mixture [21,22]. Lenz et al. [21]
435 observed a colour change from white to yellow when tablets containing physical IND-ARG were
436 immersed in the dissolution medium as well as a clear supersaturation followed by a rapid decrease
437 in IND concentration (recrystallization). In the present study, the colour change could also be
438 observed, but the PVP added to the tablet formulation possibly inhibited drug precipitation from
439 supersaturated solution.

440 Based on the dissolution profiles from the 24h dissolution study (Figure 7C), the cumulative
441 dissolved amount of IBU from the B4-formulation containing PVP remained relatively constant
442 (~34 mg or 45%) between 15min and 24h, whereas with the tablets lacking PVP only ~11 mg
443 (15%) was released after 15 min of dissolution. However, the release of IBU from tablets without
444 PVP continued throughout the study, and at 24h, the difference in cumulative dissolved amounts
445 between tablets containing and lacking PVP was no longer significant. With the N2-formulation
446 (Figure 7D), the IND release from both tablets (with and without PVP) was relatively fast (~69 mg
447 (92%) after 15 min). However, with the formulation without PVP, the dissolved amount of IND

448 began to decrease already after 15 min, and from 2h onwards it was significantly lower than with
449 the formulation containing PVP. The cumulative dissolved IND from the N2-formulation
450 containing PVP decreased only slightly during the 24h. These observations clearly indicated the
451 solubilizing and precipitation inhibitory effects of PVP. With IND the precipitation inhibitory effect
452 of PVP has been attributed to crystal growth inhibition caused by adsorption of PVP on IND
453 surfaces, whereas with IBU the solubilization is due to the strong interactions between IBU and
454 PVP [67,73-82].

455 It has also been relatively unknown, if the co-amorphous formulations maintain their dissolution
456 advantage over for example PM or amorphous drug alone, when formulated as tablets [10].
457 However, based on the present study, even a relatively small addition of stabilizing polymer as a
458 physical mixture with co-amorphous powder might stabilize the supersaturation of the amorphous
459 drug. A similar observation was made by Petry et al. [22] by coating tablets containing co-
460 amorphous IND-ARG with a polymeric coating. However, even though the film coating was
461 applied to protect the formulation from moisture, the coating process itself causes various stresses
462 (heat, moisture, mechanical) to the formulation. Thus, incorporating the polymer to the tablet
463 formulation, as shown in the present work, might be suitable also for materials that cannot
464 withstand a coating process.

465 *3.2.3 Tablet characterization*

466 The stability studies were conducted with every formulation (B1-B9 and N1-N9), but since the
467 observations from the formulations containing the same drug-ARG mixture and sugar alcohol
468 resembled each other, the X-ray diffractograms and FTIR spectra of B2-, B4-, N2- and N6-

formulation are shown here as examples (Figure 8). The diffractograms and spectra of other formulations can be found from the supplementary material (Figures S5 and S6).

At day 0, the majority of the diffractograms showed only peaks originating from either mannitol or xylitol (Figure 8A and Figures S5 and S6), which indicates that despite the possible mechanical and heat stresses [24,25], the co-amorphous salts were physically stable under compaction. Additionally, no signs of recrystallization could be observed during the 20-week stability study in the diffractograms of either the IBU-ARG formulations containing mannitol or any of the N formulations. IND-ARG has been found to be highly stable under various conditions and as a pure powder or when formulated as tablets [11,16,19,21,22]. Additionally, in our previous study [19], co-amorphous IBU-ARG did not recrystallize over one year in dry conditions, but at 60% RH liquefaction occurred. In the present study, the tablets retained their original appearance, and in the tablets containing mannitol, the IBU-ARG mixture remained amorphous. However, already at day 0, the diffractogram of B1-formulation included a small peak appeared at approximately 16.8° (2θ), which could be observed in the diffractograms of every formulation containing IBU-ARG and xylitol after 6 weeks. Additionally, a peak at approximately 19.0 ° (2θ) emerged in almost every diffractogram of these formulations. In the diffractograms from 12- and 20-week time points, these peaks became more obvious, and a peak at approximately 6.0° (2θ) began to appear.

The IR spectra between 1400-1800 cm^{-1} of all the N-formulations and the spectra of mannitol containing B-formulations corresponded to the spectra reported previously [16,19,21,72], and remained unchanged during the 20 week stability study indicating salt formation between the components as well as high physical stability (Figures 8B and S6). However, with B-formulations containing xylitol, peak shifted and new peaks appeared (Figures 8B and S5). Instead of the broad CN stretch band at 1540 cm^{-1} in the spectrum of co-amorphous IBU-ARG salt, a peak with two maxima at 1566 and 1577 cm^{-1} appeared in the spectra of the stored B1-, B2-, B5-, B6- and B9-formulations. These peaks may originate from the antisymmetric stretch of the ionized carboxylic

494 acid group of IBU as well as from the shifted CN-stretching vibration of ARG [72]. Additionally,
495 the peak at 1632 cm^{-1} (ARG guanidyl group stretching) and the shoulder at 1668 cm^{-1} (ARG COO^-
496 and guanidyl group stretching) in the IBU-ARG spectrum had shifted to a peak at 1629 cm^{-1} and to
497 a shoulder at 1657 cm^{-1}, respectively, and a new shoulder appeared at 1704 cm^{-1} (IBU carbonyl
498 stretching). With B1-, B2-, B6- and B9-formulations, these changes occurred already after 6 weeks
499 of storage, and after 20 weeks they were present also in the spectrum of the B5-formulation
500 (samples were not measured at 12 weeks).

501 The peaks appearing in the diffractograms of the B formulations containing xylitol could be
502 attributed to either crystalline IBU (peaks at 6.1°, 16.6°, 16.7° and 19.0° (2θ)) or ARG (peaks at
503 16.8° and 19.1° (2θ)) (diffractograms not shown), but the components may also have crystallized as
504 a salt, as observed by Kasten et al. [83] with IND-lysine. Additionally, Petry et al. [84] observed the
505 formation of a crystalline IND-ARG salt after storing the IND-ARG physical mixture under 75%
506 RH. However, since we have been unable to produce crystalline IBU-ARG [19], no reference
507 diffractogram of crystalline IBU-ARG salt was available. The appearance of a shoulder at 1704 cm^{-1}
508 in the IR spectra of these formulations suggest that IBU had, at least partly, recrystallized as a free
509 acid. However, due to the other spectral changes, also the crystalline IBU-ARG salt may be present
510 in the xylitol containing IBU-ARG formulations. The presence of PVP complicates the analysis
511 further, since it interacts strongly with IBU and even solid-state *in situ* amorphization has been
512 observed [73,85,86]. Thus, the exact nature of the recrystallized species could not be resolved with
513 the current methods, and the coexistence of amorphous IBU-ARG together with crystalline IBU
514 and/or ARG and/or IBU-ARG salt seemed possible. However, xylitol reduced the physical stability
515 of co-amorphous IBU-ARG, possibly due to its higher hygroscopicity when compared to mannitol
516 [51].

517 Multimodal non-linear optical imaging, specifically involving CARS and SFG/SHG, was used to
518 visualize the tablet surfaces over the 20 week period. Crystalline arginine, xylitol and mannitol

519 exhibited strong SFG/SHG signals due to their non-centrosymmetric crystal structures. L-arginine
520 has a monoclinic crystal structure with space group $P2_1$ (CSD code TAQBIY [87]) and xylitol and
521 D-mannitol have orthorhombic crystal structures with space group $P2_12_12_1$ (CSD codes
522 XYLTOL04 [88] for xylitol and DMANTL08 [89] and DMANTL09 [90] for the alpha and beta
523 polymorphs of D-mannitol, respectively) [91-93]. The spray-dried co-amorphous mixtures and
524 centrosymmetric crystalline ibuprofen and gamma indomethacin did not exhibit SFG/SHG signals
525 (data not shown). Gamma indomethacin has a triclinic structure with space group $P\bar{1}$ (CSD code
526 INDMET03 [94]) and ibuprofen has a monoclinic structure with space group $P2_1/c$ (CSD code
527 IBPRAC06 [95]) [96,97].The SFG/SHG activities of amorphous, gamma and alpha indomethacin,
528 their Raman and CARS spectra as well as the tendency of indomethacin to recrystallize to the
529 gamma-form under relatively dry conditions are known [35].

530 The CARS and Raman spectra of the co-amorphous IND-ARG mixture exhibited similarities to the
531 spectra of amorphous indomethacin with two distinguishable C=O stretching peaks at 1579 cm^{-1}
532 and 1676 cm^{-1} (Figure S7 A and B) [35,98]. Crystalline ibuprofen exhibited a distinguishable
533 CARS peak at 1603 cm^{-1} (Figure S7 B). This C-C stretching peak [99] typically moves to higher
534 Raman shifts when the ibuprofen is amorphous, for example in an amorphous solid dispersion with
535 PVP [100]. The CARS spectra of the co-amorphous mixture of IBU-ARG revealed this shift with
536 the peak at 1615 cm^{-1} (Figure S7 B and C). PVP exhibited its broad amide C=O stretching peak at
537 around 1640 – 1676 cm^{-1} (Figure S7 A and B) [101]. Xylitol and mannitol exhibited a CH_2
538 stretching peak at 1472 cm^{-1} and 1460 cm^{-1} in the CARS spectra, respectively [102] (Figure S7 A
539 and B). The CARS spectrum of arginine lacked any distinguishable peaks (Figure S7 A and B).

540 On the basis of these analyses, the distribution of different chemical components on tablet surfaces
541 could be imaged by combining CARS and SFG/SHG microscopies. Xylitol and mannitol could be
542 probed by SFG/SHG, while amorphous IND-ARG, IBU-ARG and PVP could be imaged using
543 CARS (Figure 9 and S9-13). In the images some regions appear darker than others due the surface

roughness of the tablets (the non-linear optical signal is generated only at the small focal point). Since CARS spectra were measured on tablet surfaces, it was possible to use different approaches to form images and extracted spectra from different regions could be further used to identify different chemical and solid-state components spatially. A PCA based approach was successfully used to visualize component distribution on the IBU-ARG tablet surfaces (formulations B2 and B4, Figure 9 A,D,G,I). However, the indomethacin signal from IND-ARG tablets was so dominant that a PCA based approach was not able to identify PVP (data not shown). However, PVP could be distinguished by visualizing the tablet surface using a single CARS shift at 1652 cm^{-1} (C=O stretching specific to PVP) with supportive spectral information extracted from regions of interest confirming the spectral profile of PVP (Figure S9). On the other hand spectral differences between the PVP and drug-ARG mixtures could be utilized in fast narrowband single-shift CARS imaging, together with simultaneous SFG/SHG imaging, as demonstrated in tile scan obtained from the IBU-ARG formulation B2 (Figure S10).

The CARS and SEM images (Figure 9 and Figures S9-S12 and S14) suggest that the spray dried particles were much more prominent on the surfaces of the freshly prepared tablets than could be expected based on the high mass percentage of mannitol or xylitol. Additionally, the CARS images indicated that the spray-dried particles were considerably smaller than the PVP and sugar alcohol particles, and that the sugar alcohol particles as well as PVP particles were surrounded by the spray dried particles. Barra et al. [103] reported the adherence of small excipient particles with preferable compaction properties on larger poorly compacting drug particles, which resulted in enhanced compaction properties of the mixture when compared to mixtures where no interactions existed between the drug end excipient particles. Thus, the observations on component distribution based on CARS images might have indicated a significant effect of the amount of drug-ARG mixtures on the compaction properties of the powders as well as on the mechanical properties of the tablets. However, the models predicting compaction and tablet properties suggested that the sugar alcohol

569 species was the most significant factor affecting the investigated responses and only with elastic
570 recovery, the model prediction could possibly be explained by the visual observations (i.e. coverage
571 of the sugar alcohol particles by the spray-dried particles). This discrepancy between model
572 predictions and visual observations may be explained by the small changes in the amounts of drug-
573 ARG mixtures when compared to the change of the entire sugar alcohol species. Thus, in the future,
574 it would be beneficial to perform compaction studies with larger variation in the amount of the
575 spray-dried material in order to verify the significance of the co-amorphous material on the
576 compaction process suggested by the CARS and SEM.

577 The most prominent difference between CARS/SFG/SHG images of IBU-ARG and IND-ARG
578 obtained over the 20 week period was the change in surface morphology, which was confirmed by
579 the SEM images from fresh and stored (6 months) tablets (Figures S11, S12 and S14). On day 0, the
580 co-amorphous drug-ARG particles could be clearly seen in both B- and N- formulations. However,
581 the surface of IBU-ARG tablets (B4- and B2- formulations) became smoother and individual
582 particles were not visible anymore. This change in surface morphology could be observed already
583 on week 4 (Figure S13) and smooth surface appearance remained over 20 week period (Figure 9).
584 However, CARS spectroscopy revealed that spectra extracted from tablet surfaces on day 0 and on
585 week 20 resembled closely each other in IBU-ARG formulations B4 and B2 (Figure 9) and IND-
586 ARG formulations N2 and N6 (Figure S9), thus any recrystallization in both IBU-ARG and IND-
587 ARG tablets was not observed with the non-linear optical imaging.

588 Since signs of recrystallization were observed in the B2 formulation with XRD and FTIR already
589 after 6 weeks of storage, these techniques were also used to measure the tablets imaged with CARS
590 after 14 and 20 weeks of storage (data not shown). After 14 weeks no crystallization was observed
591 with any of the formulations, but after 20 weeks a small peak at 16.9° 2θ appeared in the
592 diffractogram of B2 formulation and minor changes could also be observed in its IR spectrum. The
593 higher stability of the B2 formulation imaged with CARS when compared to the one examined with

XRD and FTIR may be due to the moisture absorption of the spray dried powder prior to the compression, which was more pronounced during the preparation of the tablets for XRD and FTIR than for the non-linear optical imaging. However, since recrystallization could also be detected with XRD and FTIR in the B2 formulation imaged with CARS, it seems that the crystallisation was limited and occurred outside the limited surface area (465x465 µm) probed with non-linear optical imaging. Detection of recrystallization with CARS may also have been compromised by the lack of reference IBU-ARG crystalline salt, although it is likely that the crystalline salt would have exhibited some CARS spectral and/or SFG signal differences compared to the amorphous form.

One main benefit of coherent Raman imaging such as CARS with SFG/SHG microscopy is the imaging speed. Tile scan shown in Figure S10 was composed of 20 1024 × 1024 pixel images acquired at two CARS shifts 1652 cm^{-1} (PVP) and 1615 cm^{-1} (IBU-ARG) with a pixel dwell time of 1.2 µs resulting in a total acquisition without laser tuning of approximately 1 min. Additionally, data-acquisition time in spectral scan was approximately 15 min, whereas it can take up to hours to perform spontaneous Raman mapping [104]. In the present study, it was shown that non-linear optical imaging is well-suited to stability analysis of formulated tablet surfaces. Nevertheless, confirming and thus imaging the chemical- and solid-state forms of different species requires non-linear optical knowledge of the crystallizing species and proper reference materials.

4. Conclusions

In the present study, tablets of sufficient strength could be produced from both co-amorphous IBU-ARG and IND-ARG salts, which also were found to be relatively physically stable during tablet compaction, even though this may be affected by the excipients. However, based on the results of the experimental design, mannitol could be recommended as a diluent for co-amorphous formulations over xylitol, since mannitol produced stronger tablets with no recrystallization in any of the formulations, whereas XRD and FTIR detected signs of recrystallization from tablets

containing IBU-ARG and xylitol. The drug release was more efficient from the tablets containing co-amorphous mixtures when compared to physical mixtures, and a small amount of PVP added to the formulation as a physical mixture was found to be effective in preventing drug recrystallisation from supersaturated solutions, which might be useful with physically stable co-amorphous mixtures that may be unable to stabilize supersaturation. In the present study, synergistic and simultaneous CARS/SFG/SHG imaging/spectroscopy was successfully used to map different chemical components on tablet surfaces. We were unable to detect phase separation or recrystallization of the co-amorphous components due to their high physical stability. Thus, due to the capability of high speed imaging of tablet surfaces, CARS and SFG/SHG are interesting options to complement the traditional XRD and FTIR in physical stability monitoring.

ACKNOWLEDGMENTS

The authors thank Microscopy laboratory at SIB Labs, University of Eastern Finland for providing laboratory facilities, PhD Jari Leskinen for SEM imaging and Master student Jarmo Maaranen for his skilful technical assistance. RO acknowledges the support from the Doctoral Programme in Drug Research in the Doctoral School of University of Eastern Finland as well as Nordforsk (NordicPOP, project number 85352). JS and CS acknowledge the Academy of Finland (project number 289398) and Business Finland (project number 462073).

APPENDIX

Supplementary data associated with this article can be found in the online version.

639 **REFERENCES**

640 [1] H.D. Williams, N.L. Trevaskis, S.A. Charman, R.M. Shanker, W.N. Charman, C.W. Pouton,
641 C.J. Porter, Strategies to address low drug solubility in discovery and development, Pharmacol.
642 Rev. 65 (2013) 315-499. doi: 10.1124/pr.112.005660.

643 [2] M. Rodriguez-Aller, D. Guillarme, J. Veuthey, R. Gurny, Strategies for formulating and
644 delivering poorly water-soluble drugs, J. Drug Deliv. Sci. Technol. 30 (2015) 342-351. doi:
645 10.1016/j.jddst.2015.05.009.

646 [3] B.C. Hancock, G. Zografi, Characteristics and Significance of the Amorphous State in
647 Pharmaceutical Systems, J. Pharm. Sci. 86 (1997) 1-12. doi: 10.1021/js9601896

648 [4] R. Laitinen, K. Löbmann, C.J. Strachan, H. Grohganz, T. Rades, Emerging trends in the
649 stabilization of amorphous drugs, Int. J. Pharm. 453 (2013) 65-79. doi:
650 10.1016/j.ijpharm.2012.04.066.

651 [5] P. Kanaujia, P. Poovizhi, W.K. Ng, R.B.H. Tan, Amorphous formulations for dissolution and
652 bioavailability enhancement of poorly soluble APIs, Powder Technol. 285 (2015) 2-15. doi:
653 10.1016/j.powtec.2015.05.012.

654 [6] K.K. Qian, R.H. Bogner, Application of mesoporous silicon dioxide and silicate in oral
655 amorphous drug delivery systems, J. Pharm. Sci. 101 (2012) 444-463. doi: 10.1002/jps.22779.

656 [7] H. Grohganz, P.A. Priemel, K. Löbmann, L.H. Nielsen, R. Laitinen, A. Mullertz, G. Van den
657 Mooter, T. Rades, Refining stability and dissolution rate of amorphous drug formulations, Expert
658 Opin. Drug Deliv. 11 (2014) 977-989. doi: 10.1517/17425247.2014.911728.

659 [8] S. Baghel, H. Cathcart, N.J. O'Reilly, Polymeric Amorphous Solid Dispersions: A Review of
660 Amorphization, Crystallization, Stabilization, Solid-State Characterization, and Aqueous
661 Solubilization of Biopharmaceutical Classification System Class II Drugs, J. Pharm. Sci. 105
662 (2016) 2527-2544. doi: 10.1016/j.xphs.2015.10.008.

663 [9] S.J. Dengale, H. Grohganz, T. Rades, K. Löbmann, Recent advances in co-amorphous drug
664 formulations, Adv. Drug Deliv. Rev. 100 (2016) 116-125. doi: 10.1016/j.addr.2015.12.009.

665 [10] R. Laitinen, K. Löbmann, H. Grohganz, P. Priemel, C.J. Strachan, T. Rades, Supersaturating
666 drug delivery systems: The potential of co-amorphous drug formulations, Int. J. Pharm. 532 (2017)
667 1-12. doi: 10.1016/j.ijpharm.2017.08.123.

668 [11] K. Löbmann, H. Grohganz, R. Laitinen, C. Strachan, T. Rades, Amino acids as co-amorphous
669 stabilizers for poorly water soluble drugs-Part 1: preparation, stability and dissolution enhancement,
670 Eur. J. Pharm. Biopharm. 85 (2013) 873-881. doi: 10.1016/j.ejpb.2013.03.014.

671 [12] R. Ojarinta, A.T. Heikkinen, E. Sievänen, R. Laitinen, Dissolution behavior of co-amorphous
672 amino acid-indomethacin mixtures: The ability of amino acids to stabilize the supersaturated state
673 of indomethacin, Eur. J. Pharm. Biopharm. 112 (2017) 85-95. doi: 10.1016/j.ejpb.2016.11.023.

674 [13] W. Wu, K. Löbmann, T. Rades, H. Grohganz, On the role of salt formation and structural
675 similarity of co-formers in co-amorphous drug delivery systems, Int. J. Pharm. 535 (2018) 86-94.
676 doi: 10.1016/j.ijpharm.2017.10.057.

677 [14] G. Craye, K. Löbmann, H. Grohganz, T. Rades, R. Laitinen, Characterization of Amorphous
678 and Co-Amorphous Simvastatin Formulations Prepared by Spray Drying, Molecules 20 (2015)
679 21532-21548. doi: 10.3390/molecules201219784.

680 [15] A. Beyer, L. Radi, H. Grohganz, K. Löbmann, T. Rades, C.S. Leopold, Preparation and
681 recrystallization behavior of spray-dried co-amorphous naproxen-indomethacin, Eur. J. Pharm.
682 Biopharm. 104 (2016) 72-81. doi: 10.1016/j.ejpb.2016.04.019.

683 [16] K.T. Jensen, L.I. Blaabjerg, E. Lenz, A. Bohr, H. Grohganz, P. Kleinebudde, T. Rades, K.
684 Löbmann, Preparation and characterization of spray-dried co-amorphous drug-amino acid salts, J.
685 Pharm. Pharmacol. 68 (2016) 615-624. doi: 10.1111/jphp.12458.

686 [17] L. Arnfast, M. Kamruzzaman, K. Löbmann, J. Aho, S. Baldursdottir, T. Rades, J. Rantanen,
687 Melt Extrusion of High-Dose Co-Amorphous Drug-Drug Combinations, Pharm. Res. (2017) 1-9.
688 doi: 10.1007/s11095-017-2254-8.

689 [18] E. Lenz, K. Löbmann, T. Rades, K. Knop, P. Kleinebudde, Hot Melt Extrusion and Spray
690 Drying of Co-amorphous Indomethacin-Arginine With Polymers, J. Pharm. Sci. 106 (2017) 302-
691 312. doi: 10.1016/j.xphs.2016.09.027.

692 [19] R. Ojarinta, L. Lerminiaux, R. Laitinen, Spray drying of poorly soluble drugs from aqueous
693 arginine solution, Int. J. Pharm. 532 (2017) 289-298. doi: 10.1016/j.ijpharm.2017.09.015.

694 [20] R.B. Chavan, R. Thipparaboina, D. Kumar, N.R. Shastri, Co amorphous systems: A product
695 development perspective, Int. J. Pharm. 515 (2016) 403-415. doi: 10.1016/j.ijpharm.2016.10.043.

696 [21] E. Lenz, K.T. Jensen, L.I. Blaabjerg, K. Knop, H. Grohganz, K. Löbmann, T. Rades, P.
697 Kleinebudde, Solid-state properties and dissolution behaviour of tablets containing co-amorphous
698 indomethacin-arginine, Eur. J. Pharm. Biopharm. 96 (2015) 44-52. doi: 10.1016/j.ejpb.2015.07.011.

699 [22] I. Petry, K. Löbmann, H. Grohganz, T. Rades, C.S. Leopold, Solid state properties and drug
700 release behavior of co-amorphous indomethacin-arginine tablets coated with Kollicoat® Protect,
701 Eur. J. Pharm. Biopharm. 119 (2017) 150-160. doi: 10.1016/j.ejpb.2017.06.007.

702 [23] Renuka, S.K. Singh, M. Gulati, R. Narang, Stable amorphous binary systems of glipizide and
703 atorvastatin powders with enhanced dissolution profiles: formulation and characterization, Pharm.
704 Dev. Technol. 22 (2017) 13-25. doi: 10.3109/10837450.2015.1125921.

705 [24] S. Patel, A.M. Kaushal, A.K. Bansal, Compression physics in the formulation development of
706 tablets, Crit. Rev. Ther. Drug Carrier Syst. 23 (2006) 1-65. doi:
707 10.1615/CritRevTherDrugCarrierSyst.v23.i1.10

708 [25] B. Demuth, Z.K. Nagy, A. Balogh, T. Vigh, G. Marosi, G. Verreck, I. Van Assche, M.E.
709 Brewster, Downstream processing of polymer-based amorphous solid dispersions to generate tablet
710 formulations, Int. J. Pharm. 486 (2015) 268-286. doi: 10.1016/j.ijpharm.2015.03.053.

711 [26] A. Agrawal, M. Dudhedia, W. Deng, K. Shepard, L. Zhong, E. Povilaitis, E. Zimny,
712 Development of Tablet Formulation of Amorphous Solid Dispersions Prepared by Hot Melt
713 Extrusion Using Quality by Design Approach, AAPS PharmSciTech 17 (2016) 214-232. doi:
714 10.1208/s12249-015-0472-0.

715 [27] P.T. Mah, D. Novakovic, J. Saarinen, S. Van Landeghem, L. Peltonen, T. Laaksonen, A.
716 Isomäki, C.J. Strachan, Elucidation of Compression-Induced Surface Crystallization in Amorphous
717 Tablets Using Sum Frequency Generation (SFG) Microscopy, Pharm. Res. 34 (2017) 957-970. doi:
718 10.1007/s11095-016-2046-6.

719 [28] N.K. Thakral, S. Mohapatra, G.A. Stephenson, R. Suryanarayanan, Compression-induced
720 crystallization of amorphous indomethacin in tablets: Characterization of spatial heterogeneity by
721 two-dimensional X-ray diffractometry, Mol. Pharm. 12 (2015) 253-263. doi: 10.1021/mp5005788.

722 [29] C.J. Strachan, M. Windbergs, H.L. Offerhaus, Pharmaceutical applications of non-linear
723 imaging, Int. J. Pharm. 417 (2011) 163-172. doi: 10.1016/j.ijpharm.2010.12.017.

724 [30] J.X. Cheng, X.S. Xie, Coherent anti-Stokes Raman scattering microscopy: Instrumentation,
725 theory, and applications, J. Phys. Chem. B 108 (2004) 827-840. doi: 10.1021/jp035693v

726 [31] P.J. Campagnola, A.C. Millard, M. Terasaki, P.E. Hoppe, C.J. Malone, W.A. Mohler, Three-
727 dimensional high-resolution second-harmonic generation imaging of endogenous structural proteins
728 in biological tissues, Biophys. J. 82 (2002) 493-508. doi: 10.1016/S0006-3495(02)75414-3.

729 [32] J.X. Cheng, X.S. Xie, Vibrational spectroscopic imaging of living systems: An emerging
730 platform for biology and medicine, Science 350 (2015) doi: 10.1126/science.aaa8870.

731 [33] J. Pirhonen, J. Arola, S. Sädevirta, P. Luukkonen, S. Karppinen, T. Pihlajaniemi, A. Isomäki,
732 M. Hukkanen, H. Yki-Järvinen, E. Ikonen, Continuous Grading of Early Fibrosis in NAFLD Using
733 Label-Free Imaging: A Proof-of-Concept Study, PLoS One 11 (2016) e0147804. doi:
734 10.1371/journal.pone.0147804.

735 [34] C.M. Hartshorn, Y.J. Lee, C.H. Camp, Z. Liu, J. Heddleston, N. Canfield, T.A. Rhodes, A.R.
736 Hight Walker, P.J. Marsac, M.T. Cicerone, Multicomponent chemical imaging of pharmaceutical
737 solid dosage forms with broadband CARS microscopy, Anal. Chem. 85 (2013) 8102-8111. doi:
738 10.1021/ac400671p.

739 [35] D. Novakovic, J. Saarinen, T. Rojalin, O. Antikainen, S.J. Fraser-Miller, T. Laaksonen, L.
740 Peltonen, A. Isomäki, C.J. Strachan, Multimodal Nonlinear Optical Imaging for Sensitive Detection
741 of Multiple Pharmaceutical Solid-State Forms and Surface Transformations, Anal. Chem. 89 (2017)
742 11460-11467. doi: 10.1021/acs.analchem.7b02639.

743 [36] A. Fussell, E. Garbacik, H. Offerhaus, P. Kleinebudde, C. Strachan, In situ dissolution analysis
744 using coherent anti-Stokes Raman scattering (CARS) and hyperspectral CARS microscopy, Eur. J.
745 Pharm. Biopharm. 85 (2013) 1141-1147. doi: 10.1016/j.ejpb.2013.08.012.

746 [37] C.J. Strachan, T. Rades, C.J. Lee, Determination of the optical second harmonic response of
747 pharmaceutical solid-solid mixtures, Opt. Lasers Eng. 43 (2005) 209-220. doi:
748 10.1016/j.optlaseng.2004.06.004.

749 [38] D. Wanapun, U.S. Kestur, L.S. Taylor, G.J. Simpson, Single Particle Nonlinear Optical
750 Imaging of Trace Crystallinity in an Organic Powder, Anal. Chem. 83 (2011) 4745-4751. doi:
751 10.1021/ac1031397.

752 [39] J.C. Parajó, H. Domínguez, J.M. Domínguez, Biotechnological production of xylitol. Part 1:
753 Interest of xylitol and fundamentals of its biosynthesis, Bioresour. Technol. 65 (1998) 191-201. doi:
754 10.1016/S0960-8524(98)00038-8.

755 [40] J. Hellrup, J. Nordström, D. Mahlin, Powder compression mechanics of spray-dried lactose
756 nanocomposites, Int. J. Pharm. 518 (2017) 1-10. doi: 10.1016/j.ijpharm.2016.12.041.

757 [41] R.C. Rowe, P.J. Sheskey, C. Owen Siân (Eds.), Handbook of Pharmaceutical Excipients, 5th
758 ed., Pharmaceutical Press and American Pharmacists Association, London, 2006.

759 [42] X. Cao, N. Leyva, S.R. Anderson, B.C. Hancock, Use of prediction methods to estimate true
760 density of active pharmaceutical ingredients, Int. J. Pharm. 355 (2008) 231-237. doi:
761 10.1016/j.ijpharm.2007.12.012.

762 [43] E. Berlin, M.J. Pallansch, Densities of several proteins and L-amino acids in the dry state. J.
763 Phys. Chem. 72 (1968) 1887-1889. doi: 10.1021/j100852a004

764 [44] M. Kuentz, H. Leuenberger, Pressure susceptibility of polymer tablets as a critical property: A
765 modified Heckel equation, J. Pharm. Sci. 88 (1999) 174-179. doi: 10.1021/js980369a.

766 [45] S. Paul, C.C. Sun, The suitability of common compressibility equations for characterizing
767 plasticity of diverse powders, Int. J. Pharm. 532 (2017) 124-130. doi:
768 10.1016/j.ijpharm.2017.08.096.

769 [46] N.A. Armstrong, R.F. Haines-Nutt, Elastic recovery and surface area changes in compacted
770 powder systems, Powder Technol. 9 (1974) 287-290. doi: 10.1016/0032-5910(74)80054-9.

771 [47] J.T. Fell, J.M. Newton, Determination of Tablet Strength by the Diametral-Compression Test,
772 J. Pharm. Sci. 59 (1970) 688-691. doi: 10.1002/jps.2600590523

773 [48] N. Willecke, A. Szepes, M. Wunderlich, J.P. Remon, C. Vervaet, T. De Beer, A novel
774 approach to support formulation design on twin screw wet granulation technology: Understanding
775 the impact of overarching excipient properties on drug product quality attributes, Int. J. Pharm. 545
776 (2018) 128-143. doi: 10.1016/j.ijpharm.2018.04.017.

777 [49] MODDE 11 User Guide, MKS Umetrics AB, Sweden

778 [50] R. Vehring, Pharmaceutical particle engineering via spray drying, Pharm. Res. 25 (2008) 999-
779 1022. doi: 10.1007/s11095-007-9475-1.

780 [51] G.K. Bolhuis, E.G. Rexwinkel, K. Zuurman, Polyols as filler-binders for disintegrating tablets
781 prepared by direct compaction, Drug Dev. Ind. Pharm. 35 (2009) 671-677. doi:
782 10.1080/03639040802587799.

[52] T. Tanner, O. Antikainen, H. Ehlers, D. Blanco, J. Yliruusi, Examining mechanical properties of various pharmaceutical excipients with the gravitation-based high-velocity compaction analysis method, Int. J. Pharm. 539 (2018) 131-138. doi: 10.1016/j.ijpharm.2018.01.048

[53] P.V. Marshall, P. York, J.Q. Maclaine, An investigation of the effect of the punch velocity on the compaction properties of ibuprofen, Powder Technol. 74 (1993) 171-177. doi: 10.1016/0032-5910(93)87009-D.

[54] L.E. Morris, J.C. Moore, J.B. Schwartz, Characterization and performance of a new direct compression excipient for chewable tablets: Xylitab®, Drug Dev. Ind. Pharm. 22 (1996) 925-932. doi: 10.3109/03639049609065922.

[55] P. Di Martino, M. Beccerica, E. Joiris, G.F. Palmieri, A. Gayot, S. Martelli, Influence of crystal habit on the compression and densification mechanism of ibuprofen, J. Cryst. Growth 243 (2002) 345-355. doi: 10.1016/S0022-0248(02)01523-3.

[56] V. Mazel, V. Busignies, H. Diarra, P. Tchoreloff, On the links between elastic constants and effective elastic behavior of pharmaceutical compacts: Importance of poisson's ratio and use of bulk modulus, J. Pharm. Sci. 102 (2013) 4009-4014. doi: 10.1002/jps.23710.

[57] A. Nokhodchi, J.L. Ford, P.H. Rowe, M.H. Rubinstein, The effects of compression rate and force on the compaction properties of different viscosity grades of hydroxypropylmethylcellulose 2208, Int. J. Pharm. 129 (1996) 21-31. doi: 10.1016/0378-5173(95)04236-9.

[58] O.F. Akande, M.H. Rubinstein, P.H. Rowe, J.L. Ford, Effect of compression speeds on the compaction properties of a 1:1 paracetamol-microcrystalline cellulose mixture prepared by single compression and by combinations of pre-compression and main-compression, Int. J. Pharm. 157 (1997) 127-136. doi: 10.1016/S0378-5173(97)00185-3.

[59] H. Larhrib, J.I. Wells, M.H. Rubinstein, Compressing polyethylene glycols: The effect of compression pressure and speed, Int. J. Pharm. 147 (1997) 199-205. doi: 10.1016/S0378-5173(96)04818-1.

[60] J. Ruangchayajatuporn, T. Amornsakchai, N. Sinchaipanid, A. Mitrevej, Compaction behavior and optimization of spray-dried lactose with various amorphous content, J. Drug Deliv. Sci. Technol. 21 (2011) 175-181. doi: 10.1016/S1773-2247(11)50019-X.

[61] N. Al-Zoubi, F. Odeh, I. Nikolakakis, Co-spray drying of metformin hydrochloride with polymers to improve compaction behavior, Powder Technol. 307 (2017) 163-174. doi: 10.1016/j.powtec.2016.11.027

[62] T. Suzuki, H. Nakagami, Effect of crystallinity of microcrystalline cellulose on the compactability and dissolution of tablets, Eur. J. Pharm. Biopharm. 47 (1999) 225-230. doi: 10.1016/S0939-6411(98)00102-7.

[63] A.R. Paradkar, B. Chauhan, S. Yamamura, A.P. Pawar, Preparation and characterization of glassy celecoxib, Drug Dev. Ind. Pharm. 29 (2003) 739-744. doi: 10.1081/DDC-120021773.

[64] A.B. Joshi, S. Patel, A.M. Kaushal, A.K. Bansal, Compaction studies of alternate solid forms of celecoxib, Adv. Powder Technol. 21 (2010) 452-460. doi: 10.1016/j.apt.2010.01.006.

[65] J. Rojas, S. Hernandez, Effect of the compaction platform on the densification parameters of tableting excipients with different deformation mechanisms, Chem. Pharm. Bull. 62 (2014) 281-287. doi: 10.1248/cpb.c13-00884.

[66] A. Forster, J. Hempenstall, T. Rades, Characterization of glass solutions of poorly water-soluble drugs produced by melt extrusion with hydrophilic amorphous polymers, J. Pharm. Pharmacol. 53 (2001) 303-315. doi: 10.1211/0022357011775532.

[67] S.A. Surwase, L. Itkonen, J. Aaltonen, D. Saville, T. Rades, L. Peltonen, C.J. Strachan, Polymer incorporation method affects the physical stability of amorphous indomethacin in aqueous suspension, Eur. J. Pharm. Biopharm. 96 (2015) 32-43. doi: 10.1016/j.ejpb.2015.06.005.

[68] R. Paus, A. Prudic, Y. Ji, Influence of excipients on solubility and dissolution of pharmaceuticals, Int. J. Pharm. 485 (2015) 277-287. doi: 10.1016/j.ijpharm.2015.03.004.

[69] R.J. Chokshi, N.H. Shah, H.K. Sandhu, A.W. Malick, H. Zia, Stabilization of low glass transition temperature indomethacin formulations: Impact of polymer-type and its concentration, J. Pharm. Sci. 97 (2008) 2286-2298. doi: 10.1002/jps.21174.

[70] W. Zhang, C. Zhang, Y. He, B. Duan, G. Yang, W. Ma, Y. Zhang, Factors Affecting the Dissolution of Indomethacin Solid Dispersions, AAPS PharmSciTech 18 (2017) 3258-3273. doi: 10.1208/s12249-017-0813-2.

[71] N.M. Najib, M. Suleiman, A. Malakh, Characteristics of the in vitro release of ibuprofen from polyvinylpyrrolidone solid dispersions, Int. J. Pharm. 32 (1986) 229-236. doi: 10.1016/0378-5173(86)90183-3.

[72] K. Löbmann, R. Laitinen, C. Strachan, T. Rades, H. Grohganz, Amino acids as co-amorphous stabilizers for poorly water-soluble drugs-Part 2: molecular interactions, Eur. J. Pharm. Biopharm. 85 (2013) 882-888. doi: 10.1016/j.ejpb.2013.03.026.

[73] M.A. El-Hinnawi, N.M. Najib, Ibuprofen-polyvinylpyrrolidone dispersions. Proton nuclear magnetic resonance and infrared studies, Int. J. Pharm. 37 (1987) 175-177. doi: 10.1016/0378-5173(87)90024-X.

[74] N.M. Najib, M.A. El-Hinnawi, M.S. Suleiman, Physicochemical characterization of ibuprofen-polyvinylpyrrolidone dispersions, Int. J. Pharm. 45 (1988) 139-144. doi: 10.1016/0378-5173(88)90042-7.

[75] Z. Gashi, R. Censi, L. Malaj, R. Gobetto, M. Mozzicafreddo, M. Angeletti, A. Masic, P. Di Martino, Differences in the interaction between aryl propionic acid derivatives and poly(vinylpyrrolidone) K30: A multi-methodological approach, J. Pharm. Sci. 98 (2009) 4216-4228. doi: 10.1002/jps.21734.

[76] L. Malaj, R. Censi, M. Mozzicafreddo, L. Pellegrino, M. Angeletti, R. Gobetto, P. Di Martino, Influence of relative humidity on the interaction between different aryl propionic acid derivatives and poly(vinylpyrrolydone) K30: Evaluation of the effect on drug bioavailability, Int. J. Pharm. 398 (2010) 61-72. doi: 10.1016/j.ijpharm.2010.07.024.

858 [77] K.P.R. Chowdary, D. Udaya Chandra, V. Parimala, M. Indira, A factorial study on formulation
859 development of ibuprofen tablets employing starch 1500 and PVP K 30, Int. J. Pharm. Sci. Res. 3
860 (2012) 189-193. doi: 10.13040/IJPSR.0975-8232.3(1).189-93

861 [78] H. Chauhan, A. Kuldipkumar, T. Barder, A. Medek, C.H. Gu, E. Atef, Correlation of
862 inhibitory effects of polymers on indomethacin precipitation in solution and amorphous solid
863 crystallization based on molecular interaction, Pharm. Res. 31 (2014) 500-515. doi:
864 10.1007/s11095-013-1178-1.

865 [79] D. Prasad, H. Chauhan, E. Atef, Amorphous stabilization and dissolution enhancement of
866 amorphous ternary solid dispersions: Combination of polymers showing drug-polymer interaction
867 for synergistic effects, J. Pharm. Sci. 103 (2014) 3511-3523. doi: 10.1002/jps.24137.

868 [80] D. Prasad, H. Chauhan, E. Atef, Role of Molecular Interactions for Synergistic Precipitation
869 Inhibition of Poorly Soluble Drug in Supersaturated Drug-Polymer-Polymer Ternary Solution, Mol.
870 Pharm. 13 (2016) 756-765. doi: 10.1021/acs.molpharmaceut.5b00655.

871 [81] D.D. Patel, B.D. Anderson, Adsorption of Polyvinylpyrrolidone and its Impact on Maintenance
872 of Aqueous Supersaturation of Indomethacin via Crystal Growth Inhibition, J. Pharm. Sci. 104
873 (2015) 2923-2933. doi: 10.1002/jps.24493.

874 [82] D. Hirai, Y. Iwao, S.I. Kimura, S. Noguchi, S. Itai, Mathematical model to analyze the
875 dissolution behavior of metastable crystals or amorphous drug accompanied with a solid-liquid
876 interface reaction, Int. J. Pharm. 522 (2017) 58-65. doi: 10.1016/j.ijpharm.2017.02.050.

877 [83] G. Kasten, K. Nouri, H. Grohganz, T. Rades, K. Löbmann, Performance comparison between
878 crystalline and co-amorphous salts of indomethacin-lysine, Int. J. Pharm. 533 (2017) 138-144. doi:
879 10.1016/j.ijpharm.2017.09.063

880 [84] I. Petry, K. Löbmann, H. Grohganz, T. Rades, C.S. Leopold, Undesired co-amorphisation of
881 indomethacin and arginine during combined storage at high humidity conditions, Int. J. Pharm. 544
882 (2018) 172-180. doi: 10.1016/j.ijpharm.2018.04.026.

883 [85] H. Sekizaki, K. Danjo, H. Eguchi, Y. Yonezawa, H. Sunada, A. Otsuka, Solid-State Interaction
884 of Ibuprofen with Polyvinylpyrrolidone, Chem. Pharm. Bull. 43 (1995) 988-993. doi:
885 10.1248/cpb.43.988.

886 [86] S. Bogdanova, I. Pajeva, P. Nikolova, I. Tsakovska, B. Müller, Interactions of
887 poly(vinylpyrrolidone) with ibuprofen and naproxen: Experimental and modeling studies, Pharm.
888 Res. 22 (2005) 806-815. doi: 10.1007/s11095-005-2598-3.

889 [87] E. Courvoisier, P.A. Williams, G. K. Lim, C.E. Hughes, K.D.M. Harris, CCDC 855058:
890 Experimental Crystal Structure Determination, 2014, doi: 10.5517/ccxprjv

891 [88] M. Woinska, S. Grabowsky, P.M. Dominiak, K. Woźniak, D. Jayatilaka, CCDC 1423912:
892 Experimental Crystal Structure Determination, 2016, doi: 10.5517/ccdc.csd.cc1jspnn

893 [89] F.R. Fronczek, H.N. Kamel, M. Slattery, CCDC 224658: Experimental Crystal Structure
894 Determination, 2014, doi: 10.5517/cc7js1k

[90] F.R.Fronczek, H.N. Kamel, M. Slattery CCDC 224659: Experimental Crystal Structure Determination, 2014, DOI: 10.5517/cc7js2l

[91] E. Courvoisier, P.A. Williams, G.K. Lim, C.E. Hughes, K.D.M. Harris, The crystal structure of L-arginine, Chem. Commun. 48 (2012) 2761-2763. doi: 10.1039/c2cc17203h.

[92] M. Woinska, S. Grabowsky, P.M. Dominiak, K. Wozniak, D. Jayatilaka, Hydrogen atoms can be located accurately and precisely by x-ray crystallography, Sci. Adv. 2 (2016). doi: 10.1126/sciadv.1600192.

[93] F.R. Fronczek, H.N. Kamel, M. Slattery, Three polymorphs (alpha, beta and delta) of D-mannitol at 100 K, Acta Crystallogr. C 59 (2003) 567-560. doi: 10.1107/S0108270103018961.

[94] P.J. Cox, P.L. Manson, CCDC 217467: Experimental Crystal Structure Determination, 2014, doi: 10.5517/cc7992w

[95] K. Ostrowska, M. Kropidlowska, A. Katrusiak, CCDC 1041383: Experimental Crystal Structure Determination, 2015, doi: 10.5517/cc13yn0q

[96] P.J. Cox, P.L. Manson, gamma-indomethacin at 120 K, Acta Crystallogr. Sect. E Struct. Rep Online 59 (2003) 986-988. doi: 10.1107/S160053680301290X

[97] K. Ostrowska, M. Kropidlowska, A. Katrusiak, High-Pressure Crystallization and Structural Transformations in Compressed R,S-Ibuprofen, Cryst. Growth Des. 15 (2015) 1512-1517. doi: 10.1021/cg5018888.

[98] S.A. Surwase, J.P. Boetker, D. Saville, B.J. Boyd, K.C. Gordon, L. Peltonen, C.J. Strachan, Indomethacin: New Polymorphs of an Old Drug, Mol. Pharm. 10 (2013) 4472-4480. doi: 10.1021/mp400299a.

[99] M.L. Vueba, M.E. Pina, De Carvalho, L A E Batista, Conformational stability of ibuprofen: Assessed by DFT calculations and optical vibrational spectroscopy, J. Pharm. Sci. 97 (2008) 845-859. doi: 10.1002/jps.21007.

[100] J. Breitenbach, W. Schrof, J. Neumann, Confocal Raman-spectroscopy: Analytical approach to solid dispersions and mapping of drugs, Pharm. Res. 16 (1999) 1109-1113. doi: 10.1023/A:1018956304595.

[101] L.S. Taylor, F.W. Langkilde, G. Zografi, Fourier transform Raman spectroscopic study of the interaction of water vapor with amorphous polymers, J. Pharm. Sci. 90 (2001) 888-901. doi: 10.1002/jps.1041.

[102] S.L. Wunder, M.I. Bell, G. Zerbi, Band Broadening of CH_2 Vibrations in the Raman-Spectra of Polymethylene Chains, J. Chem. Phys. 85 (1986) 3827-3839. doi: 10.1063/1.450903.

[103] J. Barra, F. Falson-Rieg, E. Doelker, Influence of the organization of binary mixes on their compactibility, Pharm. Res. 16 (1999) 1449-1455. doi: 10.1023/A:1018967529128.

929 [104] M.N. Slipchenko, H. Chen, D.R. Ely, Y. Jung, M.T. Carvajal, J. Cheng, Vibrational imaging
930 of tablets by epi-detected stimulated Raman scattering microscopy, Analyst 135 (2010) 2613-2619.
931 doi: 10.1039/c0an00252f.

932 LIST OF FIGURES AND TABLES

933 *Tables*

934 **Table 1**. The compositions of different tablet formulations determined by DoE.

Tablet identifier	Amount of IBU-ARG (amount of IBU)	Amount of PVP	Sugar alcohol*	Tablet mass
B1	92.2 mg (50 mg)	30.7 mg	Xylitol	307.3 mg
B2	138.3 mg (75 mg)	30.7 mg	Xylitol	422.5 mg
B3	92.2 mg (50 mg)	30.7 mg	Mannitol	307.3 mg
B4	138.3 mg (75 mg)	30.7 mg	Mannitol	422.5 mg
B5	92.2 mg (50 mg)	46.1 mg	Xylitol	345.8 mg
B6	138.33 mg (75 mg)	46.1 mg	Xylitol	461.1 mg
B7	92.2 mg (50 mg)	46.1 mg	Mannitol	345.8 mg
B8	138.33 mg (75 mg)	46.1 mg	Mannitol	461.1 mg
B9	115.3 mg (62.5 mg)	38.4 mg	Xylitol	384.3 mg

Tablet identifier	Amount of IND-ARG (amount of IND)	Amount of PVP	Sugar alcohol*	Tablet mass
N1	74.3 mg (50 mg)	24.8 mg	Mannitol	247.8 mg
N2	111.5 mg (75 mg)	24.8 mg	Mannitol	340.8 mg
N3	74.3 mg (50 mg)	38.5 mg	Mannitol	282.0 mg
N4	111.5 mg (75 mg)	38.5 mg	Mannitol	375.0 mg
N5	74.3 mg (50 mg)	24.8 mg	Xylitol	247.8 mg
N6	111.5 mg (75 mg)	24.8 mg	Xylitol	340.8 mg
N7	74.3 mg (50 mg)	38.5 mg	Xylitol	282.0 mg
N8	111.5 mg (75 mg)	38.5 mg	Xylitol	375.0 mg
N9	92.9 mg (62.5 mg)	31.65 mg	Mannitol	311.4 mg

*Neither mannitol or xylitol have been shown to undertake Maillard reactions [39]

935

936 *Figures*

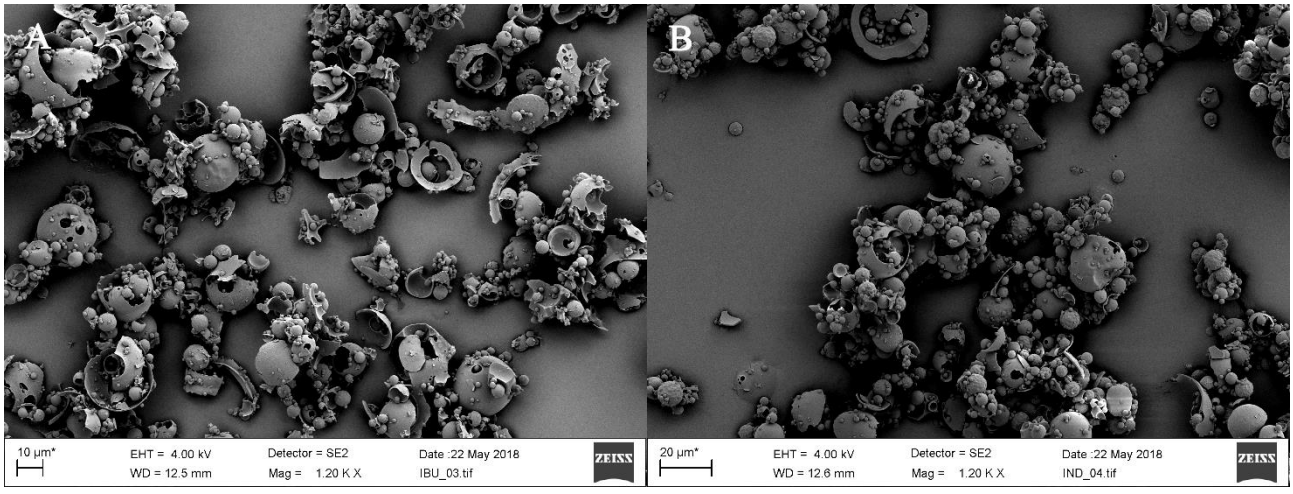

937

938 **Fig. 1.** Scanning electron microscope images of the spray dried ibuprofen-arginine (A) and

939 indomethacin-arginine (B) mixtures.

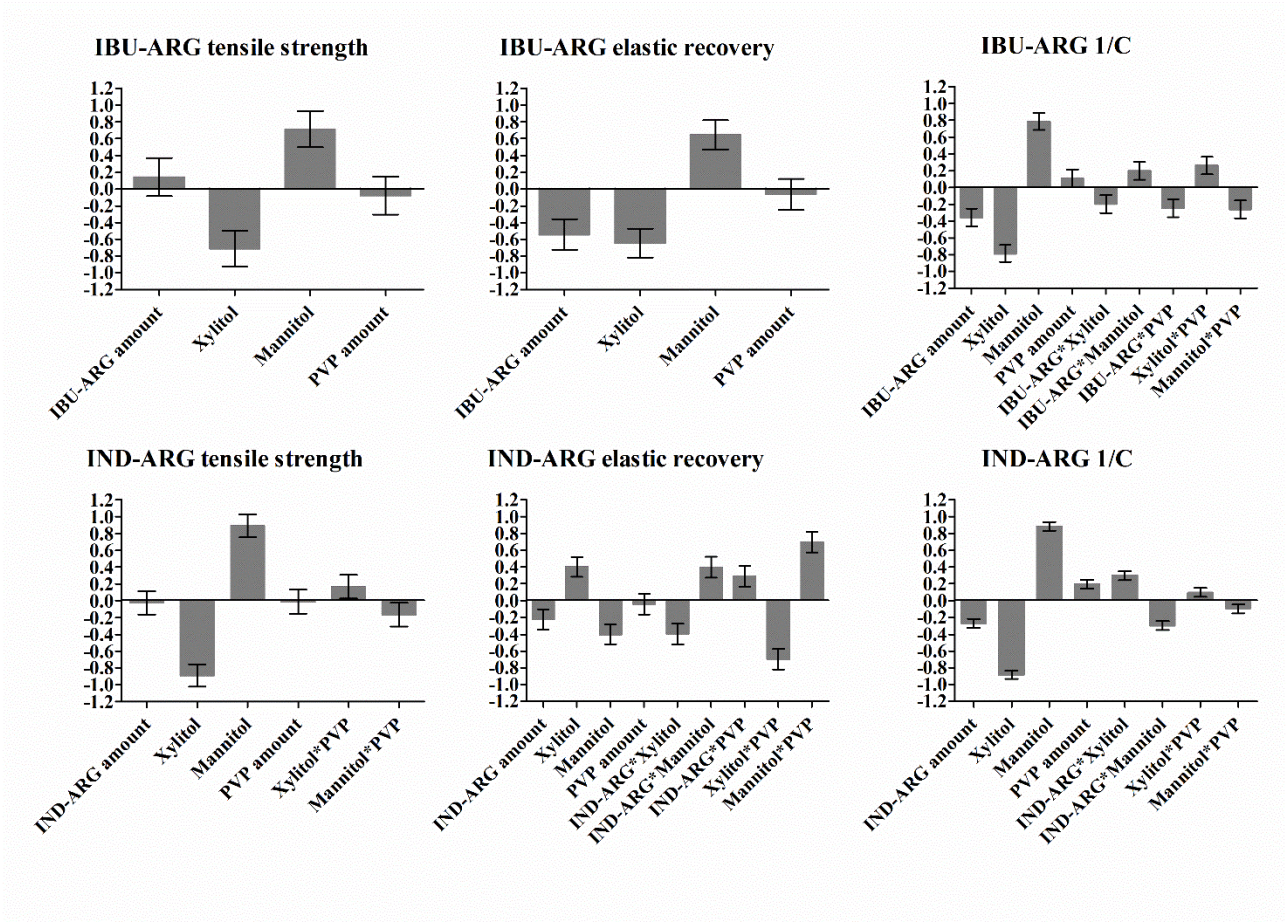

940

941 **Fig. 2.** The normalized coefficient plots of the models describing the effect of the amount of co-
942 amorphous ibuprofen-arginine (IBU-ARG) or indomethacin-arginine (IND-ARG) salt, the amount
943 of PVP and the sugar alcohol species (mannitol OR xylitol) on the mechanical properties of the
944 tablets.

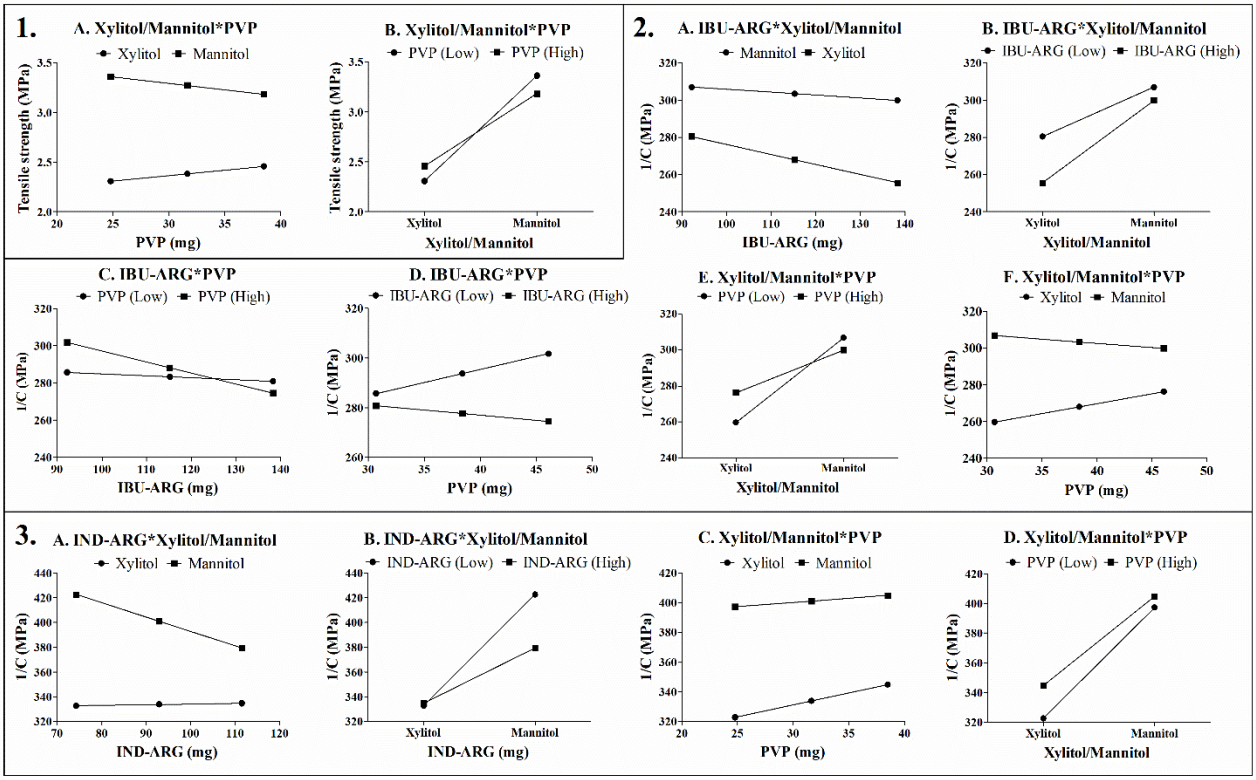

945

946 **Fig. 3.** The interaction plots of models describing the effect of changes in tablet composition on the

947 tensile strength of N formulations (1.) as well as on the 1/C value of B formulations (2.) and N

948 formulations (3.).

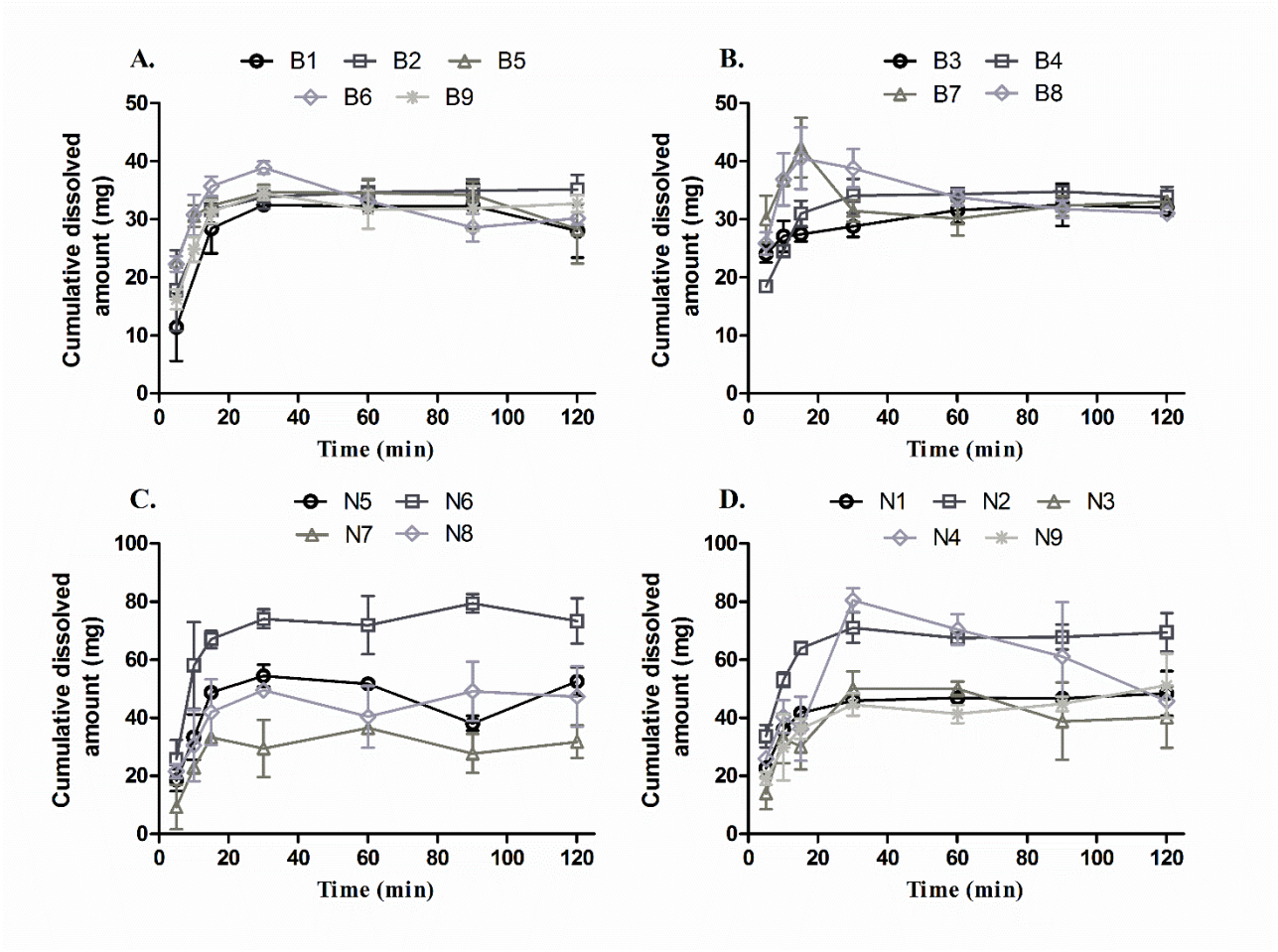

949

950 **Fig. 4.** Dissolution profiles of A. IBU-ARG and xylitol containing tablets in pH 1.2, B. IBU-ARG
951 and mannitol containing tablets in pH 1.2, C. IND-ARG and xylitol containing tablets in pH 5.0 and
952 D. IND-ARG and mannitol containing tablets in pH 5.0. The drug doses in different formulations
953 were 50 mg (B1, B3, B5, B7, N1, N3, N5, N7), 62.5 mg (B9, N9) or 75 mg (B2, B4, B6, B8, N2,
954 N4, N6, N8).

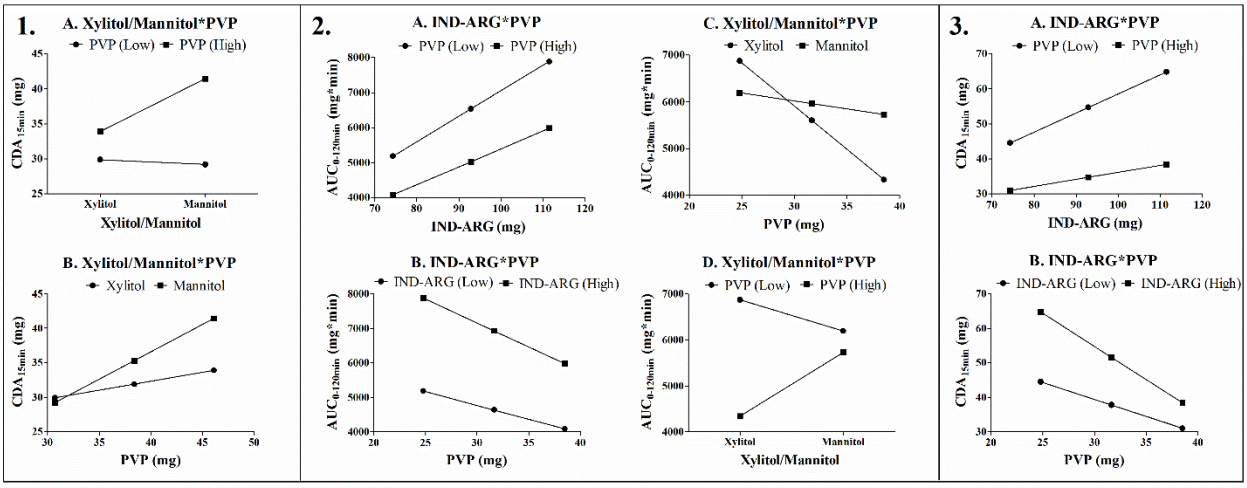

955

956 **Fig. 5.** The interaction plots of models predicting the effect of the tablet composition on the
957 CDA_{15min} of B formulations (1.) as well as on the $AUC_{0\text{-}120min}$ (2.) and CDA_{15min} (3.) of N
958 formulations.

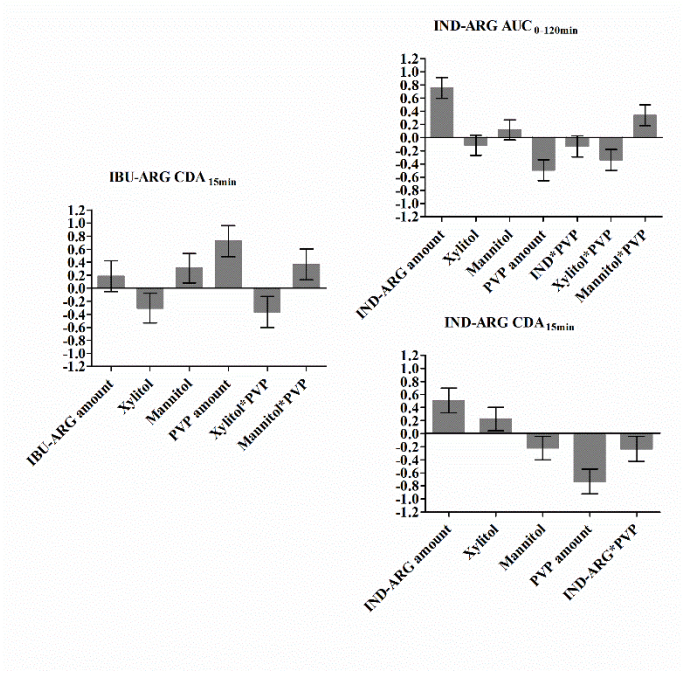

959

960 **Fig. 6.** The normalized coefficient plots of the models describing the effect of the amount of co-
961 amorphous ibuprofen-arginine (IBU-ARG) or indomethacin-arginine (IND-ARG) salt, the amount
962 of PVP and the sugar alcohol species (mannitol or xylitol) on the area under the cumulative
963 dissolved drug amount-time curve between 0 and 120 minutes (AUC0-120min) and on the
964 cumulative dissolved drug amount after 15 minutes (CDA15min).

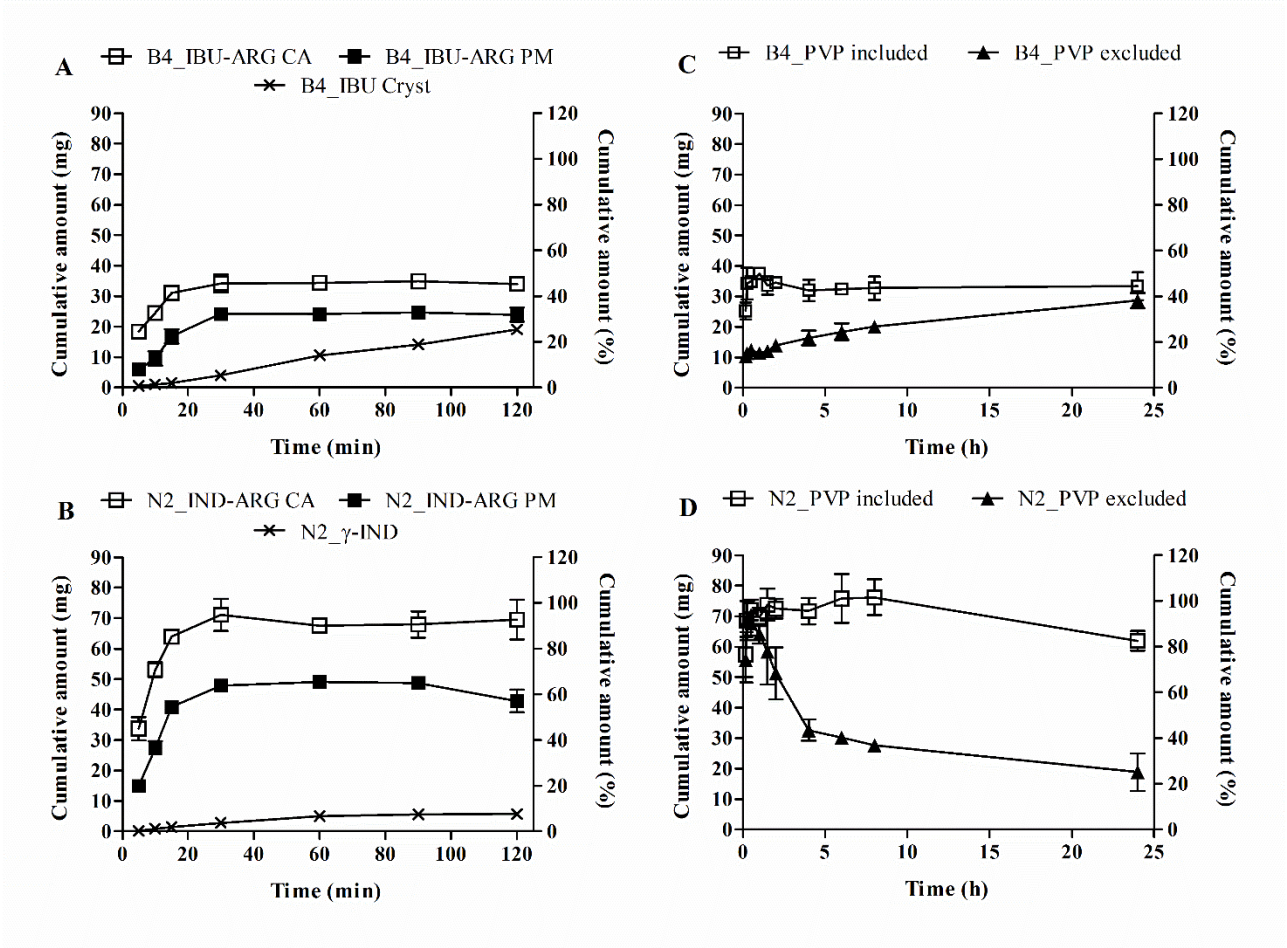

965

966 **Fig. 7.** The investigation of the effect of arginine (ARG) and the formation of co-amorphous salt
967 (CA) on the release of ibuprofen (IBU) and indomethacin (IND) from B4- and N2-formulations (A
968 and B, respectively) as well as the effect of polyvinylpyrrolidone K30 (PVP) on the supersaturation
969 stability after drug release from B4- and N2-formulations (C and D, respectively). PM denotes
970 physical mixture and Cryst crystalline drug.

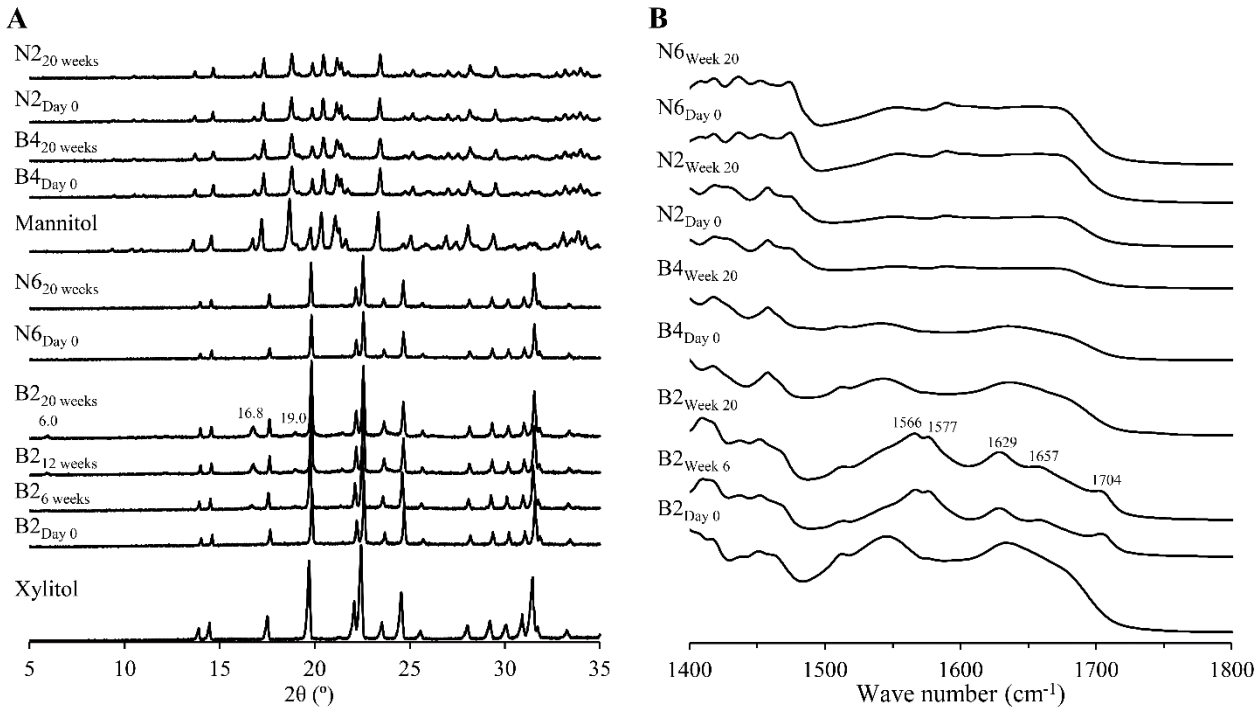

971

972 **Fig. 8.** The X-ray diffractograms (A) an FTIR spectra (B) of B2-, B4-, N2- and N6-formulations at
973 day 0 and after storage under ambient temperature and 33% relative humidity. With formulations
974 that showed no signs of recrystallization, only the data from the beginning and end of the study are
975 shown, but with B2 formulation the data from several time points is included. The diffractograms of
976 mannitol and xylitol are also included for comparison.

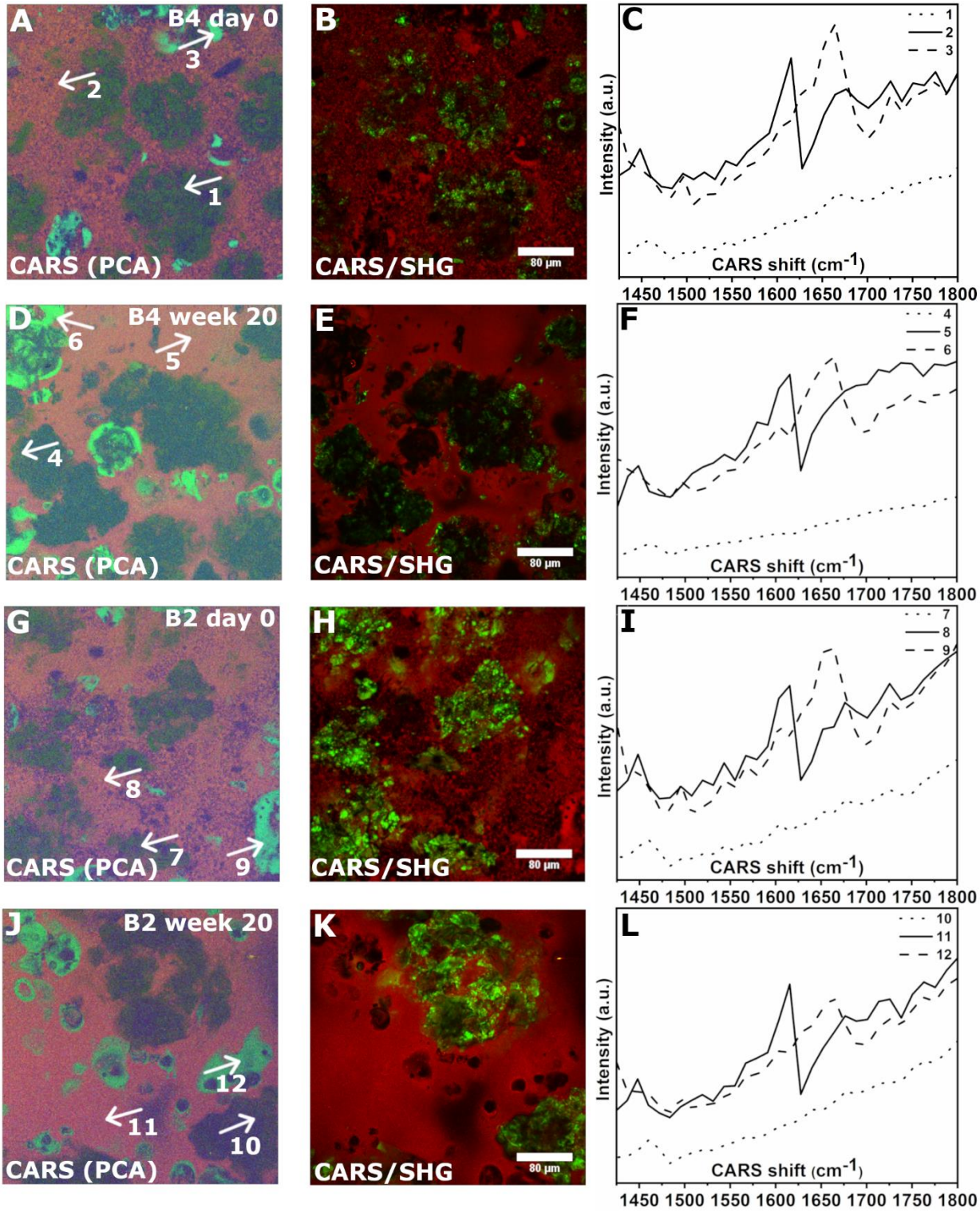

977

978 **Fig. 9.** The PCA based CARS images of tablet surfaces of B4- and B2- formulations (left column,
979 A,D,G,J), corresponding the overlaid CARS/SFG/SHG images (at 1652 cm^{-1}) (middle column,
980 B,E,H,K) and CARS spectra extracted from regions marked with white arrows and numbers (right
981 column, C,F,I,L) on day 0 and on week 20. The PCA RGB image is generated from a CARS

spectral scan in the region 1417−1804 cm^{-1}, using the score values of the first three PCs. PCA loadings are shown in Figure S8. The scale bar is 80 µm.